Agricultural and Forest Meteorology

Sensitivity Analysis of a Source Partitioning Method for H_2O and CO_2 Fluxes Based on High Frequency Eddy Covariance Data: Findings from Field Data and Large Eddy Simulations

A. Klosterhalfen[a], A.F. Moene[b], M. Schmidt[a], T.M. Scanlon[c], H. Vereecken[a], A. Graf[a]

Anne Klosterhalfen, a.klosterhalfen@fz-juelich.de, corresponding author
Arnold F. Moene, arnold.moene@wur.nl
Marius Schmidt, ma.schmidt@fz-juelich.de
Todd M. Scanlon, tms2v@virginia.edu
Harry Vereecken, h.vereecken@fz-juelich.de
Alexander Graf, a.graf@fz-juelich.de

[a] Agrosphere Institute, IBG-3, Forschungszentrum Jülich GmbH, 52425 Jülich, Germany

[b] Meteorology and Air Quality Group, Wageningen University and Research, 6708 PB Wageningen, the Netherlands

[c] Department of Environmental Sciences, University of Virginia, Charlottesville, VA 22904, United States

ABSTRACT

Scanlon and Sahu (2008) and Scanlon and Kustas (2010) proposed a source partitioning method (SK10 in the following) to estimate contributions of transpiration, evaporation, photosynthesis, and respiration to H_2O and CO_2 fluxes obtained by the eddy covariance method. High frequency eddy covariance raw data time series are needed, and the source partitioning is estimated based on separate application of the flux-variance similarity theory to stomatal and non-stomatal components of the regarded fluxes, as well as on additional assumptions on leaf-level water use efficiency (WUE).

We applied SK10 to data from two test sites (forest and cropland) and analyzed partitioning results depending on various ways to estimate WUE from available data. Also, we conducted large eddy simulations (LES), simulating the turbulent transport of H_2O and CO_2 for contrasting vertical distributions of the canopy sinks/sources, as well as for varying relative magnitudes of soil sources and canopy sinks/sources. SK10 was applied to the synthetic high frequency data generated by LES and the effects of canopy type, measurement height, given sink-source-distributions, and input of varying WUEs were tested regarding the partitioning performance. SK10 requires that the correlation coefficient between stomatal and non-stomatal scalar fluctuations is determined by the ratio of the transfer efficiencies of these scalar components, an assumption (transfer assumption in the following) that could be tested with the generated LES data.

The partitioning results of the field sites yielded satisfactory flux fractions, when fair-weather conditions (no precipitation) and a high productive state of the vegetation were present. Further, partitioning performance with regard to soil fluxes increased with crop maturity. Results also showed relatively large dependencies on WUE, where the partitioning factors (median) changed by around -57% and +36%. Measurements of outgoing longwave radiation used for the estimation of foliage temperature and WUE could slightly increase the

plausibility of the partitioning results in comparison to soil respiration measurements by decreasing the partitioning factor by up to 42%. The LES-based analysis revealed that for a satisfying performance of SK10, a certain degree of decorrelation of the H_2O and CO_2 fluctuations (here, $|\rho_{q'c'}| < 0.975$) was needed. This decorrelation is enhanced by a clear separation between soil sources and canopy sinks/sources, and for observations within the roughness sublayer. The expected dependence of the partitioning results on the WUE input could be observed. However, due to violation of the abovementioned transfer assumption, the known true input WUE did not yield the known true input partitioning. This could only be achieved after introducing correction factors for the transfer assumption, which were known however only in the special case of the LES experiments.

Keywords: Flux Partitioning, Latent Heat Flux, LES, Net Ecosystem Exchange, Sensitivity Analysis, Water Use Efficiency

1. Introduction

The eddy covariance (EC) method is a convenient measurement technique for energy, water vapor, and carbon dioxide exchange between atmosphere and biosphere. It is routinely used for a better understanding of the exchange of greenhouse gases, providing, among others, fluxes of H_2O and CO_2 based on high-resolution (10 - 20 Hz) raw data of the concentrations of these gases and the vertical wind velocity. The method yields net fluxes; to gain deeper insight into the underlying biophysical processes, source partitioning methods have to be applied to the data to distinguish between the fluxes from the various compartments of the biosphere. Measured net ecosystem exchange (NEE) of CO_2 and its two components gross primary production (GPP) and total ecosystem respiration (TER) are of particular interest (Reichstein et al. 2012; Stoy et al. 2006b). In addition, elements of the water cycle, their dynamics, and magnitudes have to be considered to comprehend the interrelation between atmosphere and terrestrial systems more completely. Particularly the study of evapotranspiration (ET), with its two components evaporation (E) and transpiration (T), and its feedbacks with the carbon cycle should be incorporated in environmental studies (Scanlon and Kustas 2010).

A large variety of source partitioning procedures with diverse approaches and necessity of different input data have been developed (Kool et al. 2014; Reichstein et al. 2012; Stoy et al. 2006a, 2006b). The most popular partitioning tools for CO_2 flux components, primarily developed to fill gaps in EC measurements of NEE, are often based on the notion that during night respiration fluxes dominate. They use regressed relationships of EC measurements (typically averaged over half-hourly periods) and physical drivers, in particular temperature (e.g., approach after Reichstein et al. 2005). The approach after Lasslop et al. (2010) additionally constrains the rate of photosynthesis with light response curves from daytime flux measurements. Similar to these CO_2 gap-filling models, ET can be partitioned via time

intervals with an inactive canopy (without any T), such as for croplands shortly after harvest, in deciduous forests after leaf fall, or for some canopy types due to low air temperatures (Reichstein et al. 2012; Stoy et al. 2006a). However, such source partitioning approaches are well developed for the partitioning of carbon fluxes, but analogous and established methods for water fluxes are lacking yet (Reichstein et al. 2012; Stoy et al. 2006a, 2006b). Instrumental approaches of source partitioning require, next to EC data, additional measurements at different parts of ecosystems and with different methods, e.g., soil-flux chamber measurements, profile measurements (Ney and Graf 2018), or tracer measurements (isotopes). The latter are promising for flux partitioning, but associated with high costs, elaborate technical setups, and maintenance requirements that are usually not possible at most stations (Kool et al. 2014; Reichstein et al. 2012). With flux chambers, sap flux sensors, and microlysimeters sources and sinks of H_2O and/or CO_2 can be derived in an ecosystem, but are associated with scaling issues in comparison to the EC footprint.

As a data-driven method only requiring existing data from a typical EC station, Scanlon and Sahu (2008) and Scanlon and Kustas (2010) proposed a method to estimate the contributions of T, E, photosynthesis, and soil respiration (R_s, autotrophic and heterotrophic sources) using measured high frequency time series of water vapor and CO_2 concentrations. This method (further called SK10) is based on the dissimilarities of sources and sinks of water vapor and CO_2 among sub-canopy, canopy, and atmosphere, which lead to unique "signals" in EC measurements for air transported from differing locations. The flux-variance similarity theory is separately applied to the stomatal and non-stomatal components of the regarded scalars. The discrepancy between the perfect correlation between H_2O and CO_2 exchange at leaf-level (via the water use efficiency WUE) and the imperfect correlation between H_2O and CO_2 fluctuations above the canopy is used to determine the relative strength of each flux component. SK10 requires that the correlation coefficient between stomatal and non-stomatal

scalar fluctuations is determined by the ratio of the transfer efficiencies of these scalar components, an assumption (transfer assumption in the following) made by Scanlon and Sahu (2008) in the method's derivation.

Scanlon and Kustas (2012) applied SK10 to a maize field (eastern USA) and showed that the performance of ET partitioning is consistent, can give insights for calculation of canopy conductance, and therefore, has the potential to improve land surface models. A comparison between isotopic H_2O flux partitioning and SK10 was conducted by Good et al. (2014). Wang et al. (2016) analyzed H_2O flux partitioning by SK10 at a suburban grassland site (western USA), that yielded similar diurnal and seasonal dynamics compared to simulations with the Noah Land Surface Model. Sulman et al. (2016) compared SK10 with other partitioning methods (sub-canopy EC measurements, non-linear regression method, and potential evapotranspiration) and evaluated its performance in a forest site in a decadal time scale. Considering ten day moving averages the multiple methods showed a good agreement for T and GPP and a higher variability in E and TER.

Sulman et al. (2016) suggested further investigation of SK10 via large eddy simulation (LES) studies identifying potential sources of errors in the application of the partitioning method. Various LES studies including a canopy have been conducted studying the influence of canopy properties and canopy edges on airflow above and in the canopy (e.g., Cassiani et al. 2008; Dupont and Brunet 2008; Finnigan et al. 2009). Huang et al. (2013) studied the influence of coherent structures on the scalar dissimilarity in the air space just above the canopy via LES. They investigated the scalar-scalar-correlation in forest canopies with differing densities. Edburg et al. (2012) simulated the transport of passive scalars for a forest canopy and concluded that scalar concentration profiles, fluxes, correlation coefficients, and scalar segregation are affected by the sink-source-distribution of the scalars. We assumed that these differing characteristics also influence the performance of SK10.

In spite of the partly successful applications of SK10 (see above), the method is still not widely used and robustness issues have been reported (mostly personal communication). We aim to identify the key assumptions behind the method that, if not properly met, can lead to its failure. To this end, we applied the partitioning method to data of two contrasting field sites with various WUE assumptions derivable from meteorological measurements. Furthermore, we applied SK10 to data obtained on synthetic high frequency data by LES, checked scalar statistics, the validity of the transfer assumption, and evaluated the partitioning method.

2. Materials and Methods

2.1. Study Sites

The measurements were obtained at Selhausen (50°51'N, 6°26'E, 103 m a.s.l., ICOS code DE-RuS) and Wüstebach (50°30'N, 6°19'E, 610 m a.s.l., ICOS code DE-RuW) in western Germany. These study sites are included in the Terrestrial Environmental Observatories (TERENO) network of highly instrumented field sites.

Selhausen is located in the southern part of the Lower Rhine Embayment. The underlying sediments are Quaternary fluvial deposits from the Rhine/Meuse and Rur river system and were covered by floodplain sediments and loess in the Pleistocene and Holocene. The major soil type was classified as a Luvisol according to the soil taxonomy of the FAO (I.U.S.S. Working Group WRB 2006). The soil texture is a silt loam and fairly homogeneous in the area (Weihermüller et al. 2007). The climate conditions are temperate maritime with a mean annual temperature of 9.9 °C and an annual precipitation of 698 mm (1961-2009; Graf et al. 2012). The dominant land-use in the region is cropland and in 2015 winter wheat (*Triticum aestivum* L.) was cultivated in Selhausen. The crop height was between 0.57 and 0.81 m and the effective (Chen 1996) leaf area index (LAI) based on optical measurements was between 5.7 and 6.8 m^2 m^{-2} on the considered days. EC measurements (measurement height 2.43 m) and ancillary environmental measurements were conducted in the center of the field with an area of approximately 9.8 ha. Measurements of H_2O, CO_2, wind components, sensible heat, global radiation, air temperature, precipitation, and relative humidity were available for the regarded time periods. A detailed description of the measurement setups is given by Ney and Graf (2018). All observations were averaged in half-hourly time steps, while the measurement frequency of the EC method was 20 Hz. Here, we use the micrometeorological convention, where downward fluxes from atmosphere to biosphere are negative and upward fluxes positive (Stoy et al. 2006b).

196 The Wüstebach catchment is part of the low mountain range Eifel and covers an area of
197 ~38.5 ha; the altitude ranges from 595 m to 628 m a.s.l. The underlying bedrock consists of
198 fractured Devonian slate with sporadic sandstone inclusions. Soil types vary from Cambisols
199 and Planosols to Gleysols and Histosols depending on the average groundwater level. Soil
200 texture is a silty clay loam (Bogena et al. 2015). The mean annual temperature is 7.5 °C and
201 the annual precipitation is 1220 mm (1979-1999; Bogena et al. 2015; Ney et al. unpublished
202 data). The dominant vegetation type is Norway spruce (*Picea abis* L.). EC and ancillary
203 environmental measurements (same as in Selhausen) were taken in a height of 38 m above
204 ground, over a spruce canopy of 25 m height and a LAI of about 3.9 m^2 m^{-2} (Ney et al.
205 unpublished data).
206 SK10 is applied to half-hourly time series of pre-processed high frequency EC data of vertical
207 wind velocity, total H_2O, and CO_2 concentrations. Beforehand, physically implausible values
208 and spikes were excluded in the high frequency data, the time delay was corrected, missing
209 raw data within one 30 minutes period was gap-filled by linear interpolation and a planar-fit
210 rotation was conducted.
211 For the application of the source partitioning method, days with a high productive state of the
212 vegetation and fair-weather conditions (sunny, almost no precipitation, clear diurnal dynamics
213 of all meteorological variables) were chosen to ensure that all flux components contributed to
214 the measured total fluxes and to exclude processes and factors further disturbing the
215 stationarity of turbulence and the expected behavior of the stomata (e.g., cloud cover). Also,
216 the method was only applied to time periods where the quality assessment scheme during EC
217 processing (after Mauder et al. 2013) assigned the highest or intermediate out of three quality
218 flag levels. Furthermore, for Selhausen half-hour periods have been excluded if the relative
219 contribution of the target field to the footprint (after Kormann and Meixner 2001) was smaller
220 than 80%. For Wüstebach time periods with wind directions between 70° and 162° were

excluded to receive only flux measurements of the desired target area (cf. Graf et al. 2014 for a cumulative footprint analysis). Furthermore, the source partitioning method was merely applied to daytime data because the SK10 method requires the presence of photosynthesis. Here, sunrise and sunset times were calculated by means of local time, and in addition, daytime was designated to a measured global radiation higher than 20 W m^{-2} after Reichstein et al. (2005).

For validation purposes, soil respiration data were obtained with closed-chamber measurements at both sites ($R_{s\text{-}meas}$). In Selhausen, half-hourly measurements of an automated soil gas efflux system (LI-8100, Li-Cor Inc. Biosciences, Lincoln, NE, USA) with four stationary longterm-chambers were available for the considered time periods (Ney and Graf 2018). In Wüstebach, $R_{s\text{-}meas}$ was measured with portable survey-chambers at several measurement points in the forest on June 10th, 2015 (9 a.m. - 1 p.m.), so a spatial and temporal average for that day could be calculated. In both cases, identical PVC collars were permanently inserted 5 cm deep and 2 cm protruding above the surface into the soil; automated chambers closed on these collars only during measurement. Furthermore, soil evaporation E_{soil} was estimated as a fraction of measured ET based on Beer's law depending on LAI (E_{soil} = ET exp(-0.6 LAI); Campbell and Norman 1998; Denmead et al. 1996; Kool et al. 2014; Stoy et al. 2006a) to compare to the partitioned H_2O components by SK10 at both study sites.

2.2. Source Partitioning Based on High Frequency Data - SK10

The source partitioning method after Scanlon and Sahu (2008) and Scanlon and Kustas (2010) is based, among others, on the Monin-Obukhov similarity theory (MOST). In the atmospheric surface layer above a horizontally homogenous surface, scalar statistics in a particular height are expected to depend on the surface fluxes, surface shear stress, and buoyancy determined

by sensible and latent heat flux (Scanlon and Kustas 2010; Scanlon and Sahu 2008). Strictly, MOST implies that scalar time series measured at the same position in the atmospheric surface layer should correlate perfectly, which is consistent with the concept of flux-variance similarity (Hill 1989). These expectations are not always met under field conditions because of a non-steadiness of time series, the influence of entrainment, and heterogeneous distribution of sinks and sources (Scanlon and Kustas 2010; Scanlon and Sahu 2008).

With the EC method, high frequency measurements of water vapor and CO_2 concentrations are collected and their turbulence-driven dynamics are monitored. During the day T and photosynthesis are usually the main contributors to measured H_2O and CO_2 fluxes, and both derive from stomatal exchange. In the absence of non-stationarity and entrainment, the correlation coefficient $\rho_{q_t'c_p'}$, between the two stomatal scalars is equal to -1 according to the flux-variance similarity theory (subscripts q_t and c_p indicate moisture and CO_2 concentrations related to T and photosynthesis; likewise, subscripts q_e and c_r indicate moisture and CO_2 concentrations related to E and R_s, respectively). This relationship between H_2O loss and CO_2 uptake on leaf-level by vegetation is described by the WUE. When in a hypothetical case the fluctuations of H_2O and CO_2 (R_s and E from the soil surface disregarded) are plotted against each other, they would correlate perfectly and the linear slope would be equivalent to the WUE (WUE is defined to be negative, see Eq. 4; Scanlon and Kustas 2010; Scanlon and Sahu 2008), from which follows:

$$c_p' = \mathrm{WUE} \cdot q_t' \quad (1)$$

The non-stomatal processes, E from the soil surface and R_s, are expected to also adhere to flux-variance similarity. These fluxes originate primarily from the sub-canopy, are enriched in both H_2O and CO_2, and it is assumed that they are transported similarly with one another, but

different from the stomatal components. Since both fluxes are positive during daytime, they correlate positively and $\rho_{q_e'c_r'}$ would be equal to +1 (Scanlon and Kustas 2010; Scanlon and Sahu 2008).

For the natural case in which both stomatal and non-stomatal processes contribute to the fluxes, the correlation between water vapor fluctuations (*q'*) and CO_2 fluctuations (*c'*) is reduced. The slope of the *q'* versus *c'* relationship becomes less than WUE, such that the magnitude of the ecosystem-level WUE (WUE_{eco}, the ratio between NEE and ET) is smaller (less negative) than WUE at leaf-level (Palatella et al. 2014). The reduced correlation and deviation from WUE at leaf-level provides information about the composition and magnitudes of the measured fluxes (Scanlon and Kustas 2010; Scanlon and Sahu 2008). Scanlon and Sahu (2008) state that, to obtain accurate source partitioning from this extra information, the vegetation has to be distributed homogeneously in a horizontal sense and the vertical heterogeneity and spatial distribution of stomatal and non-stomatal sinks and sources have to be significant to reduce the degree of correlation.

The first step in the SK10 time series analysis is the correction for density fluctuations in the raw data of H_2O and CO_2 fluxes. Such fluctuations can arise due to external factors such as changes in air temperature or water vapor density. Scanlon and Kustas (2010) use the approach after Detto and Katul (2007). As mentioned before, the correlation between *q'* and *c'* is very sensitive to advection, entrainment, and large-scale weather effects. Therefore, large-scale fluctuations should be eliminated from measurements, in this case, by orthonormal wavelet transform using the discrete Haar wavelet. For 20 Hz data sets of 30 minutes (36000 data points) 15 wavelet levels can be derived (2^{15} data points in the first 27.3 min; Scanlon and Albertson 2001). In this study, the first two wavelet levels representing the low frequency eddies have always been removed by default to reduce the influence of large-scale processes as suggested by Scanlon and Kustas (2010). In the process of finding a valid solution,

additional wavelet levels can be excluded progressively, if necessary (see below). The application of wavelet transform gives an insight, how $\rho_{q'c'}$, WUE_{eco}, and scalar transport efficiencies vary across scales of turbulent eddies. The derived eddy frequencies could be converted to eddy diameters using Taylor's frozen turbulence hypothesis (Scanlon and Kustas 2010).

Figure 8 in Scanlon and Sahu (2008, page 10) shows an overview of the main analysis steps of SK10. To compute the exact combination of flux contributions, Scanlon and Sahu (2008) derived a system of equations for this approach, in which most parameters ($\overline{w'q'}$, $\overline{w'c'}$, $\rho_{q'c'}$, $\rho_{w'q'}$, $\rho_{w'c'}$, σ_q^2, σ_c^2) are known from measurements. To further reduce the number of unknowns, the following equations are assumed to be reasonable approximations (transfer assumption; Bink and Meesters 1997; Katul et al. 1995; Scanlon and Kustas 2010; Scanlon and Sahu 2008):

$$\rho_{q_t'q_e'} \approx \frac{\rho_{w'q_e'}}{\rho_{w'q_t'}} \quad (2)$$

$$\rho_{c_p'c_r'} \approx \frac{\rho_{w'c_r'}}{\rho_{w'c_p'}} \quad (3)$$

where w' is the vertical wind fluctuation. These equations imply that transport efficiencies of q_e' and c_r' coming from the soil surface are smaller than the efficiencies of q_t' and c_p' from the canopy airspace, respectively, because $|\rho_{q_t'q_e'}|$ and $|\rho_{c_p'c_r'}|$ should be smaller than 1 (Bink and Meesters 1997). This is consistent with the results of Lamaud and Irvine (2006) and Moene and Schüttemeyer (2008) who found that for the scalar pair temperature-humidity the relative transport efficiency $\rho_{w'\theta'}/\rho_{w'q'}$ is equal to $\rho_{\theta'q'}$ for well-watered conditions (small heat flux) and $1/\rho_{\theta'q'}$ for dry conditions (small moisture flux). They also show that in general $\rho_{w'\theta'}/\rho_{w'q'}$ can be described as $(\rho_{\theta'q'})^k$ with k ranging between -1 and 1.

Besides, WUE can be estimated (see below), such that only two parameters in the essential equation of the approach (Scanlon and Sahu 2008, Equation 15, page 5; Eq. A.1 in Appendix) are unknown: the correlation coefficient of the CO_2 concentrations related to photosynthesis and R_s ($\rho_{c_p'c_r'}$) and the variance of photosynthesis-related CO_2 ($\sigma_{c_p}^2$). The equation can be further manipulated to solve for $\sigma_{c_p}^2 = f(\rho_{c_p'c_r'})$ (Eq. A.2). To obtain results for $\sigma_{c_p}^2$ and the corresponding magnitudes of each flux component, values of $\rho_{c_p'c_r'}$ in a physically meaningful range of $-1 \leq \rho_{c_p'c_r'} \leq 0$ are inserted into the function. To obtain the exact partitioning solution, $\rho_{q'c'}$ is derived as a function of $\rho_{c_p'c_r'}$ and the other variables. If this calculated $\rho_{q'c'}$ matches the observed $\rho_{q'c'}$, (misfit is less than 0.005), then actual values for $\rho_{c_p'c_r'}$, $\sigma_{c_p}^2$ and the partitioning factors are found (Scanlon and Kustas 2010; Scanlon and Sahu 2008). As a further check, WUE is calculated again as a function of the derived partitioning factors and compared to the input WUE. If those 'input' and 'control' WUEs differ too much (misfit larger than 1%), the solution is disregarded. If no solution for $\rho_{c_p'c_r'}$ and $\sigma_{c_p}^2$ is attained, the next wavelet level is removed progressively to further reduce the influence of large-scale processes until a valid solution is reached or none at all. The estimated partitioning factors are then applied to the post-processed half-hourly EC data.

For a detailed analytical description of SK10 see Palatella et al. (2014), Scanlon and Albertson (2001), Scanlon and Kustas (2010, 2012), and Scanlon and Sahu (2008). Our implementation deviates from the procedure of Palatella et al. (2014) and Scanlon and Kustas (2010) in terms of finding valid solutions with a minimal error in $\rho_{q'c'}$ and WUE. Because we converted Equation 15 in Scanlon and Sahu (2008) solving for $\sigma_{c_p}^2$ directly (see Appendix A), we were left with only one unknown variable: $\rho_{c_p'c_r'}$. By insisting upon very low errors in $\rho_{q'c'}$ and WUE we found almost always the same solutions as the approach after Palatella et al. (2014), even though we passed on the implementation of the globally convergent Newton's method. Aside from this, Skaggs et al. (2018) developed an algebraic solution simplifying the

source partitioning procedure and implemented SK10 in the open source Python 3 module Fluxpart. Using the analytical approach would not significantly change our results, but it might improve the rate of convergence to a solution.

One disadvantage of SK10 is that the autotrophic CO_2 source term (growth and maintenance respiration by plants) cannot be quantified. Thus, not GPP but the above-ground net primary production (NPP; GPP minus above-ground respiration by autotrophs) is result of this approach. Furthermore, SK10 can only be applied to daytime fluxes, because it is based on the assumptions that photosynthesis is active and E positive.

Water Use Efficiency

A key element of the source partitioning method after Scanlon and Kustas (2010) is the WUE at the leaf level, which describes the relation between the amount of CO_2 uptake through stomata (photosynthesis) and the corresponding amount of H_2O loss (T) (not to be confused with WUE_{eco}, the ratio of NEE to ET).

One way to derive WUE is to relate the difference in mean CO_2 concentration between air (just outside the leaf) and stomata to the difference in mean humidity concentration between air and stomata:

$$\mathrm{WUE} = 0.7 \cdot \frac{c_s - c_i}{q_s - q_i} \quad (4)$$

where the subscripts “s” and “i” indicate the external (within canopy) and internal (intra-stomatal) concentration of H_2O (q) and CO_2 (c) averaged over the regarded time period. The factor 0.7 accounts for the difference in diffusion and convection between H_2O and CO_2 through the stomatal aperture (Campbell and Norman 1998). c_i should be lower than c_s to

maintain CO_2 uptake and q_i larger (saturated) than q_s, leading to a negative fraction (Scanlon and Kustas 2010, 2012; Scanlon and Sahu 2008).

As mentioned before, WUE should be evaluated for the leaf-level, where the exchange between plants and atmosphere takes place. c_s and q_s at displacement height can be inferred from EC measurements by considering logarithmic mean concentration profiles implementing MOST (Scanlon and Kustas 2010, 2012; Scanlon and Sahu 2008). For c_i a constant value of 270 ppm was presumed, a typical value for C3 plants (Špunda et al. 2005; Williams et al. 1996; Xue et al. 2004). Values for q_i were estimated based on 100% relative humidity at foliage temperature (T_f). Direct measurements of T_f are usually not available; therefore, Scanlon and Sahu (2008) suggested to use mean air temperature to estimate WUE (WUE_{meanT}), as well as to consider a range for T_f of 2 K lower and higher than air temperature ($WUE_{meanT-2K}$ or $WUE_{meanT+2K}$, respectively). Additionally, to investigate the sensitivity of WUE, T_f was derived by means of measured outgoing longwave radiation (WUE_{OLR}; with a surface emissivity of 0.98), or calculated similar to c_s and q_s by considering a logarithmic mean profile implementing MOST (WUE_{MOST}).

Because the chosen inputs of c_i and T_f introduce uncertainty, we conducted two additional runs with quantities of c_i and T_f on the outer margins of their reasonable ranges for a very low or very high WUE, respectively. Following Equation 4, if c_i and/or T_f (and with it q_i) increases, the magnitude of WUE decreases (WUE gets less negative), and the plant is assumed to be less efficient. For Norway spruce Špunda et al. (2005) calculated values of c_i between 180 and 400 ppm based on measured air CO_2, assimilation rate and stomatal conductance in a diurnal cycle. Xue et al. (2004) measured c_i for four different winter wheat cultivars under differing conditions and obtained a range between 120 and 300 ppm. Here, 200 and 300 ppm were chosen for a minimal or maximal magnitude of c_i, respectively. The calculated T_f by means of measured outgoing longwave radiation was during the day about

3 K or 6 K higher at the forest or crop site, respectively, than the mean air temperature. Thus, for a minimal value, q_i was calculated based on the mean air temperature minus 2 K and for a maximal value, based on air temperature plus 5 K. For the two additional applications of SK10 to the study sites, on the one hand the small values of c_i and T_f were chosen for a maximal magnitude of WUE (WUE_{MAX}) and on the other hand the larger values for a minimal magnitude of WUE (WUE_{MIN}) (Tab. 1). Note that tentatively choosing even more extreme values for c_i or T_f mostly led to no valid solutions of the SK10 procedure.

2.3. Large Eddy Simulations

LES were undertaken to study the impact of different canopy types on the vertical exchange of scalars. The effect of the vertical scalar sink-source-distribution and of the relative importance of canopy and soil source on correlation coefficients were of interest. The simulations have been performed with the Dutch Atmospheric Large-Eddy Simulation (DALES) model (Heus et al. 2010; Ouwersloot et al. 2016). The default version was extended to enable closer control of the source distribution in the canopy.

We conducted experiments with neutral flow conditions (i.e., all scalars are passive with respect to buoyancy). A frictionless rigid lid (zero-gradient boundary conditions for horizontal velocity components and all scalars, and w = 0) was applied as upper boundary condition. A periodic boundary condition was set in each horizontal direction for both velocity and all scalars. The external forcing was a constant horizontal pressure gradient. This setup was slightly different from the variable momentum forcing (targeting a constant mean velocity) used in the studies conducted by Ouwersloot et al. (2016) and Edburg et al. (2012).

A domain size of $72\ h_c \times 36\ h_c \times 32\ h_c$ with $720 \times 360 \times 144$ nodes in the x-, y-, and z-directions with a grid resolution of 0.1 canopy heights (h_c) was used for the numerical

418 experiments. In the vertical direction the grid cells were equally spaced up to a height of five
419 times the h_c and above stretched progressively to a total domain height of 32 times the h_c.
420 The total simulation runtime for each experiment was 720 $h_c\ u_*^{-1}$ (u_* is the friction velocity at
421 the canopy top), of which the last 120 $h_c\ u_*^{-1}$ were sampled. For the statistics of turbulence
422 profiles, quantities were sampled every 1 $h_c\ u_*^{-1}$ and averaged over 120 $h_c\ u_*^{-1}$, respectively.
423 Fields of momentum and scalars were sampled every 6 $h_c\ u_*^{-1}$. The Courant-Friedrichs-Lewy
424 (CFL) number was smaller than 0.5 for all runs. The time steps and the maximum horizontal
425 velocity in x-direction were variable in these simulations, but were in average about
426 0.0042 $h_c\ u_*^{-1}$ and 0.46 $h_c\ u_*^{-1}$, respectively[1].
427 The plant area density (PAD) profile was prescribed, with a smooth transition at the top of the
428 canopy over four grid points, and the canopy was resolved vertically by 10 grid points, both
429 as recommended by Ouwersloot et al. (2016). The drag coefficient C_d was set to 0.5
430 describing the drag on the flow induced by canopy elements, and we prescribed the roughness
431 length of the underlying soil as z_0 = 0.005 m. The canopy was homogeneous in the horizontal
432 direction.
433 Two LES experiments with contrasting PAD profiles were conducted: on the one hand with a
434 canopy similar to a crop (winter wheat) and on the other hand with a canopy similar to a
435 coniferous forest (Fig. 1). These canopy profiles were taken from measurements at our study
436 sites and literature (Edburg et al. 2012; Gspaltl et al. 2013; Weiskittel et al. 2009). The LAI
437 was set to 2 $m^2\ m^{-2}$ in both cases, which is a typical magnitude for forests, while winter wheat
438 usually has a considerably denser canopy. In the following, only results of the experiment
439 with the crop-like canopy are shown. The corresponding figures of the experiments with
440 forest-like canopy can be found in the Supplementary material.

[1] In dimensional terms, the various simulation characteristics are: h_c = 1 m, u_* = 0.2 m s^{-1}, total simulation run time 3600 s, of which the last 600 s were sampled; time steps and the maximum horizontal velocity in x-direction were in average about 0.021 s and 2.3 m s^{-1}, respectively.

In the simulations passive scalars were emitted homogeneously from the soil surface and from ten canopy sources (one for each grid cell in vertical direction). So, in total eleven fields of arbitrary scalars were simulated. Each of these fields can be scaled with a desired source strength for the respective source level. A scalar with sources at multiple levels can be constructed by adding these fluctuation fields, each scaled with a height-specific source strength derived from a desired vertical source strength distribution. This could be repeated for an arbitrary number of scalars and vertical source distributions after the actual LES runs. Thus, fields for both H_2O and CO_2 were created, assuming a water vapor source and a carbon sink in the canopy and a source for both scalars at the soil surface. Two different variations of distributions were applied: on the one hand a v-shaped distribution taken from Sellers et al. (1992) (ModelV, Fig. 1 left) and on the other hand a beta-function-shaped distribution inferred from profile measurements in winter barley on June 9th, 2016 (Ney et al. 2017; Ney and Graf 2018) (ModelB, Fig. 1 right). Finally, the relative strength of the CO_2 soil source was varied: the soil sources were set to 1 mmol m^{-2} s^{-1} for H_2O and to 3 or 9 µmol m^{-2} s^{-1}, respectively, for CO_2. The total flux at canopy top was for each distribution the same and matched EC measurements of the same day in June 2016 (ET = 9.2 mmol m^{-2} s^{-1}, NEE = -27.26 µmol m^{-2} s^{-1}). So, in total we had for each canopy type four different combinations of sink-source-distributions: ModelV with low or higher CO_2 soil source and ModelB with low or higher CO_2 soil source. This setup was chosen to study the influence of the separation between soil sources and canopy sink/source and of their relative magnitudes on scalar-scalar-correlations and flux profiles. Also, the impact of differing magnitudes of WUE_{eco} and WUE at canopy-level could be studied. WUE_{eco} was for all LES experiments identical, and the WUE on canopy-level did not differ between ModelV and ModelB under identical soil source strength. Furthermore, the setup allowed to separately study and compare

465 the effect of the different PADs and the resulting turbulence on the one hand, and of differing
466 scalar sink-source-distributions on the other hand.
467 After scaling the scalar fields with the chosen sink-source-distributions, variances and
468 covariances could be sampled from the LES experiments in any chosen virtual measurement
469 height. To calculate the required fluxes, simulation data of vertical wind and scalar
470 concentrations were sampled from each field (fields collected every $6\ h_c\ u_*^{-1}$ in the last
471 $120\ h_c\ u_*^{-1}$ of runtime) for every tenth grid point in x- and y-direction in each corresponding
472 height, so data for one virtual measurement height consisted of 51840 data points. After
473 calculating the necessary H_2O and CO_2 fluxes, the variances and correlation of *q'* and *c'*, and
474 WUE, the SK10 approach could be applied to this 'virtual EC data'. SK10 was only applied
475 to the resolved scale (scales of motion larger than the grid scale) statistics, assuming any
476 correlation structure found in the resolved scale would be valid for the subgrid scale (scales of
477 motion smaller than the grid scale) as well. The source partitioning results could then be
478 validated to the known fluxes and statistics of the components q_t, q_e, c_p, and c_r from the LES
479 experiments.

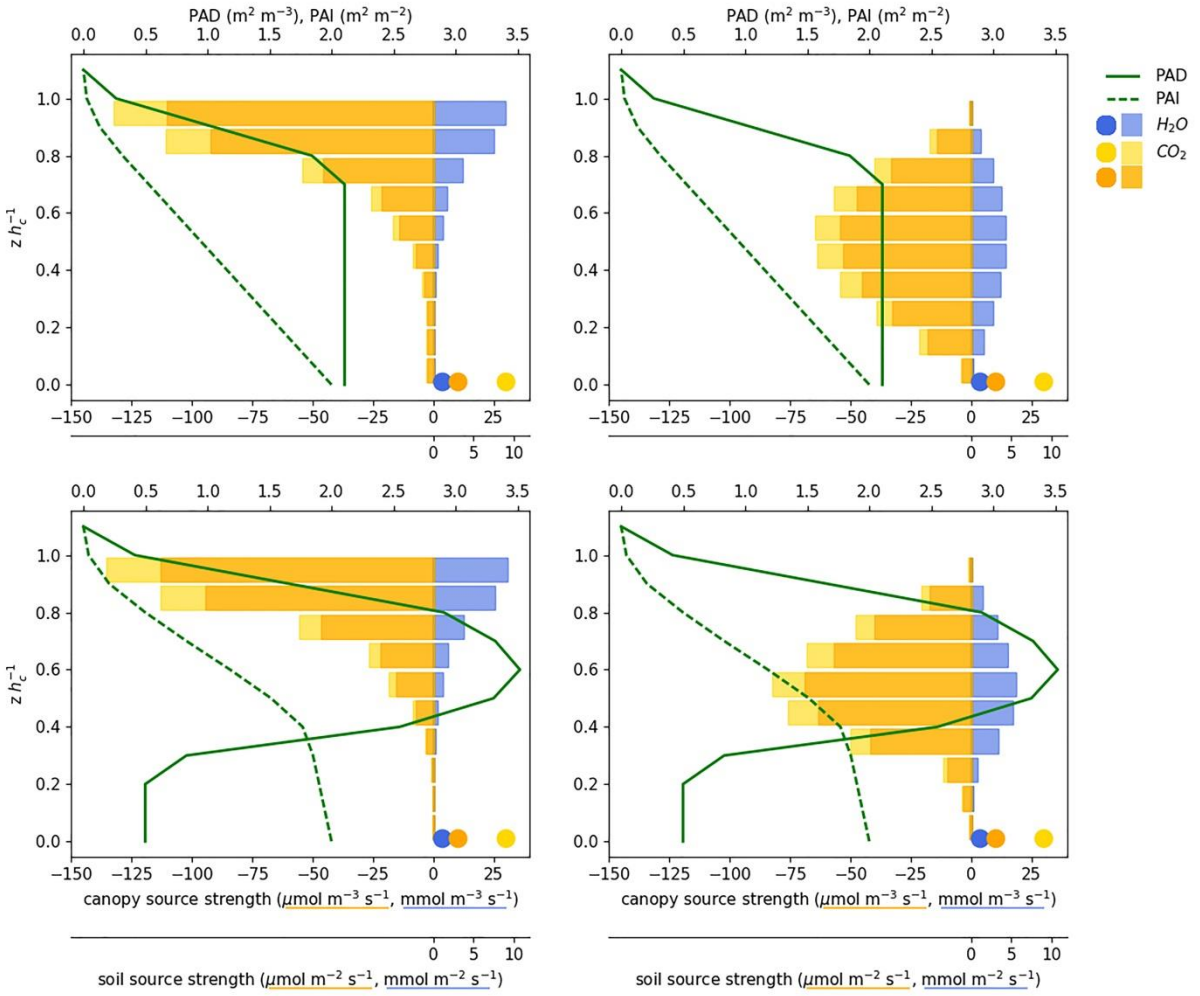

Fig. 1: Vertical profiles of the crop (*top*) and forest (*bottom*) plant area density (PAD), cumulative plant area index (PAI), and variations of sink-source-distributions for H_2O and CO_2 used to scale the LES scalar fields (*left*: ModelV, after Sellers et al. 1992; *right*: ModelB, after Ney et al. 2017), each with ten canopy sinks/sources (*bars*) and one soil source (*circle*). For CO_2, two different soil sources and accordingly differing canopy sinks were used, in which the flux at canopy top for each distribution is the same.

3. Results and Discussion

The first objective of our study was the application of SK10 to data of our study sites and the analysis of the partitioning results depending of the WUE input. The second objective was the application of SK10 to synthetic high frequency data generated by LES and the analysis of the partitioning performance depending on canopy type, measurement height, and given sink-source-distribution. Also here, dependence of the partitioning result to the WUE input was analyzed. Of particular interest was the assessment of the transfer assumption involved in SK10 (Eq. 2, 3), which was only possible with the LES experiments.

3.1 Source Partitioning of Field Data

The selected time period for the forest site included 247 daytime hours and the three periods for the cropland 359 daytime hours in total. After checking the data quality (excluding periods with precipitation events, worst quality flag, and insufficient fraction of footprint on target area) SK10 could be applied to 70% and 86% of these daytime hours for the forest and cropland site, respectively. Subsequently, SK10 found valid partitioning solutions for 75% and 58% of these high-quality daytime periods for the forest and cropland site.

Figures 2 and 3 show source partitioning results of SK10 for H_2O and CO_2 fluxes at the two study sites for certain time periods. The partitioned H_2O fluxes were compared to estimated E_{soil} computed as a fraction of measured ET based on Beer's law depending on LAI (Fig. 2; Campbell and Norman 1998; Denmead et al. 1996; Kool et al. 2014). The partitioned CO_2 fluxes were compared to results of the approach after Reichstein et al. (2005) and to $R_{s\text{-}meas}$ from chamber measurements (Fig. 3). The root mean square error (RMSE) and the bias between measured and SK10-based R_s are given in Table 1. For the calculation of the error quantities, outliers were excluded which deviated from the mean by more than ten times the standard deviation. Concerning the different chamber measurement setups, one area average

from four chamber measurements was given per considered half-hour at the crop site, while at the forest site only one space-time average from 36 consecutive manual chamber measurements in different locations was assumed to be approximately applicable for June 10th, 2015 from 9 a.m. till 1 p.m.

SK10 reasonably partitioned water vapor fluxes into larger fractions of T than E (Fig. 2). The comparison between E and estimated E_{soil} based on Beer's law showed a good agreement for the forest and larger discrepancies for the cropland. For the latter, SK10 tended to overestimate E up to tenfold in most time periods and matched the magnitude of E_{soil} perfectly in only a few time periods, keeping in mind that E_{soil} was also just an approximation. The large variations in E decreased with maturity of the crop. The median of the partitioning fraction E/ET was 0.16 for the forest and between 0.09 and 0.23 for the cropland in the three time periods. With the differing WUE inputs the median of the partitioning fractions changed by up to -57% and +29%. At the forest site E/ET (with WUE_{meanT}) increased to a median of 0.29 on the two days after the precipitation events during the night from June 12th to June 13th. Thereby, T was reduced due to an increased q_s and a decreased humidity gradient at leaf-level. This effect was also observed by Scanlon and Kustas (2012). Kool et al. (2014) reviewed 52 studies about ET partitioning and found values of E/ET between 0.05 and 0.53 for forests and between 0.1 and 0.9 for winter wheat depending on the crop cover, in which our findings belonged to the lower ranges.

Results of the CO_2 partitioning showed more scatter at both study sites (Fig. 3). While the partitioning model after Reichstein et al. (2005) has different target flux components than SK10, its respiration (TER) can be used as an upper limit for the validation of the SK10-based R_s. Here, R_s often exceeded TER (correspondingly NPP exceeded GPP) and chamber measurements, and peaked in implausible magnitudes, especially in the cropland for the two chosen time periods earlier in the year. In the latter time period, when the winter wheat

matured, NEE measurements decreased and SK10 results appeared more reasonable. Compared to $R_{s\text{-}meas}$, the estimated soil source by SK10 matched measurements very well on June 30th, but was often underestimated in early July. In the three considered time periods, weather conditions were similar and only WUE_{eco} differed. The medians of WUE_{eco} were -13.3, -9.1, and -7.3 mg g^{-1} for these three time periods, and thus the crop became less efficient with maturity. T and NPP results particularly differed between the last two time periods, which were similar in plant height and LAI, but differed in maturity of the crop. A direct relationship of T and NPP to plant height or LAI could not be observed, also because these canopy properties only varied slightly between the considered time periods (Fig. 2, 3). At the forest site, the obtained CO_2 flux components had a reasonable magnitude, except after the precipitation events. The significant increase of the flux components could be caused by the presence of interception, so the SK10 procedure could not differentiate between T and evaporation of interception water, thus, overestimating T and NPP with an unchanged WUE. The median of the partitioning fraction R_s/NEE was -0.29 for the forest and between -0.74 and -0.14 for the cropland. With the differing WUE inputs the median of the partitioning fractions changed by up to -42% and +36%.

Reasons for the diverging results of SK10 and reference estimates at our study sites could include a wrong functioning of the partitioning method, such as finding a wrong solution for $\rho_{c_p'c_r'}$, excluding not enough/too many levels of large-scale fluctuations, or an inaccurate WUE estimation. Also, invalidity of assumptions underlying the method, such as a non-identical sink-source-distribution of H_2O and CO_2 fluxes, horizontal canopy heterogeneity, insufficient vertical spacing between stomatal and non-stomatal processes, and deviations of these processes from flux-variance similarity theory, could cause the improbable results. Also, not all processes could be incorporated in the method, such as respiratory fluxes of a forest understory or woody tissue and refixation of respiratory CO_2 in the canopy.

562 The correct exclusion of large-scale fluctuations was checked with a modified SK10 method
563 by searching for the best solution in all eddy scales and not stopping at the first valid solution.
564 This did not improve partitioning results significantly (not shown). Thus, we assumed that the
565 application of the wavelet transform and the exclusion of low frequency processes were
566 efficient. By removing large-scale fluctuations, it was assumed that the removed part had a
567 composition of H_2O and CO_2 that was proportional to the remaining data (Scanlon and Sahu
568 2008). At our cropland site, the fraction of the H_2O and CO_2 fluxes transported by large-scale
569 eddies was usually smaller than 10% and very similar between water vapor and CO_2. The
570 number of removed wavelet levels for each time step decreased from an average of 6 to 3
571 levels with maturity of the crop. At our forest site, the proportions of the fluxes were larger
572 for low frequency processes (but usually smaller than 0.15) and some differences between
573 H_2O and CO_2 fractions were observed, but the partitioning performance did not seem to be
574 dependent. But the spikes in the CO_2 components observed before the precipitation events at
575 the forest site were provoked by the removal of more than ten wavelet levels in these time
576 steps, so flux fractions were not represented realistically anymore and the partitioning method
577 could not work properly.
578 As observed by Scanlon and Albertson (2001), at our forest site the largest proportions of the
579 vertical H_2O and CO_2 fluxes were also mostly transported by eddies in the order of four times
580 the canopy height. At the cropland site, the eddies transporting the largest flux fractions were
581 up to ten or even more times larger than the canopy. This and the very small distance between
582 canopy and soil surface sink/sources (relative to the measurement height) could cause the
583 unsatisfactory performance of SK10 for the cropland. Besides, EC measurements were
584 obtained at between 3 and 4.3 h_c at the crop site on the considered days and at 1.52 h_c at the
585 forest site. Assuming the roughness sublayer ranges up to 1.5 to 3 h_c (Williams et al. 2007),
586 measurements at the latter site were more likely obtained within or close to the roughness

sublayer, resulting in a lower scalar-scalar-correlation $\rho_{q'c'}$ and more information for SK10. At both study sites degraded $\rho_{q'c'}$ were observed for the excluded large-scale eddies, e.g., due to entrainment, and for eddy scales smaller than the canopy height, so $\rho_{q'c'}$ was possibly influenced by the sink-source-distribution (Huang et al. 2013; Scanlon and Sahu 2008; Williams et al. 2007). The signals were well correlated at the intermediate scales.

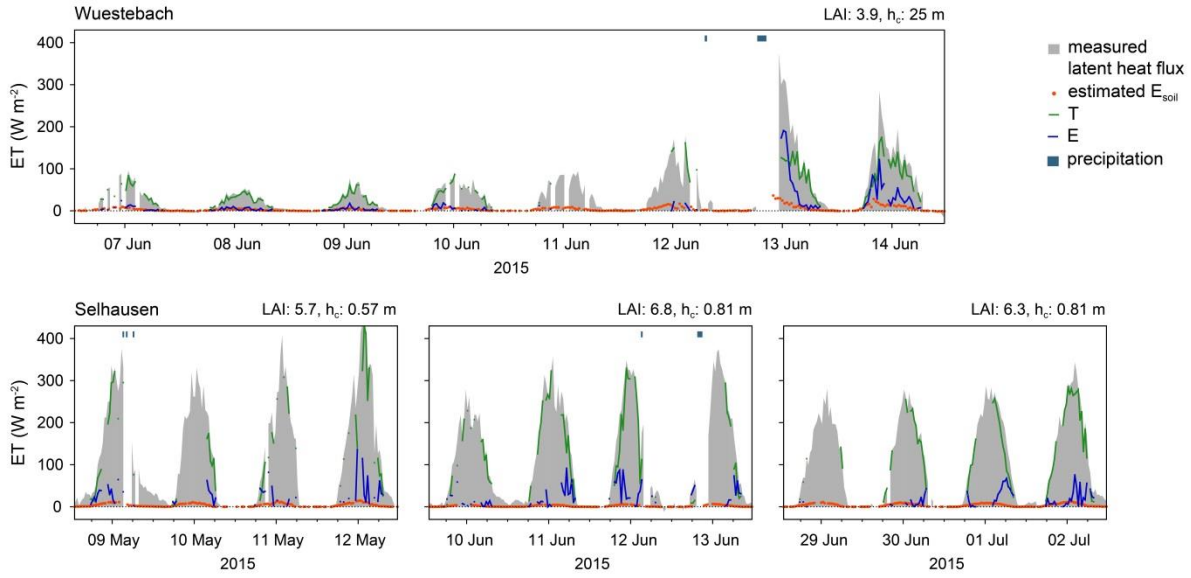

Fig. 2: Source partitioning results of the approach after Scanlon and Kustas (2010) for H_2O fluxes at the two study sites Wüstebach (forest; *top*) and Selhausen (cropland; *bottom*) for varying time periods. For the estimation of water use efficiency on leaf-level the applied foliage temperature was assumed to be equal to mean air temperature (ET: evapotranspiration; T: transpiration; E: evaporation; E_{soil}: soil evaporation calculated based on Beer's law depending on LAI; LAI: leaf area index; h_c: canopy height).

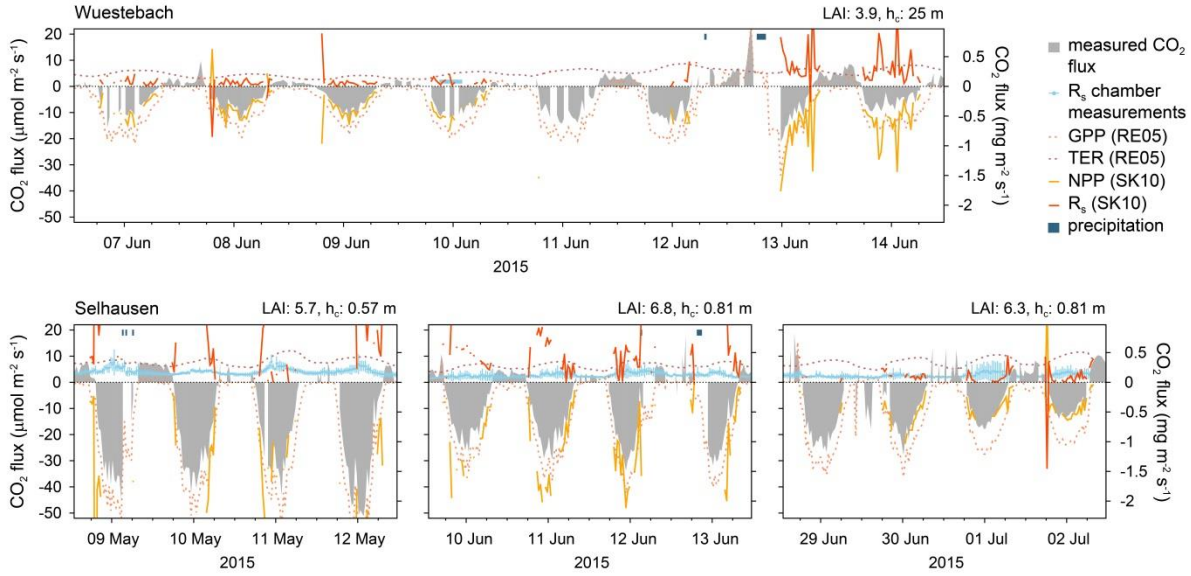

Fig. 3: Comparison of source partitioning results of the approaches after Reichstein et al. (2005, RE05) and after Scanlon and Kustas (2010, SK10) for CO_2 fluxes at the two study sites Wüstebach (forest; *top*) and Selhausen (cropland; *bottom*) for varying time periods. For the estimation of water use efficiency on leaf-level the applied foliage temperature was assumed to be equal to mean air temperature (GPP: gross primary production; NPP: net primary production; TER: total ecosystem respiration; R_s: soil respiration; LAI: leaf area index; h_c: canopy height). *Light blue bar* in Wüstebach on June 10th, 2015 shows time-space-average of R_s chamber measurements.

Tab. 1: Root mean square error (RMSE), bias in µmol m^{-2} s^{-1}, and number of found solutions (N) of source partitioning results for soil respiration after the approach of Scanlon and Kustas (2010) with various water use efficiencies (WUE; including input parameters for WUE estimation: T_f: foliage temperature; c_i: internal CO_2 concentration; meanT: measured mean air temperature; MOST: Monin-Obukhov similarity theory; OLR: outgoing longwave radiation; see Section *Water Use Efficiency* for description) compared to chamber measurements at the two study sites Selhausen (cropland) and Wüstebach (forest). Outliers were excluded which deviated from the mean by more than ten times the standard deviation.

	T_f	c_i (ppm)	Selhausen, cropland			Wüstebach, forest		
			RMSE	bias	N*	RMSE	bias	N*
$WUE_{mean\ T}$	meanT	270	16.77	6.810	184	1.39	-0.255	7
$WUE_{mean\ T\ -2\ K}$	meanT – 2 K	270	27.69	5.459	215	1.55	0.510	8
$WUE_{mean\ T\ +2\ K}$	meanT + 2 K	270	19.70	0.052	215	9.81	-7.806	8
WUE_{MOST}	via MOST	270	14.37	5.909	174	1.07	-0.876	5
WUE_{OLR}	via OLR	270	18.56	5.068	142	0.87	-0.866	3
WUE_{MAX}	meanT – 2 K	200	36.62	14.895	163	NaN	NaN	0
WUE_{MIN}	meanT + 5 K	300	26.76	3.460	114	NaN	NaN	0

* number of time steps with available chamber measurements: 280 in Selhausen, 8 in Wüstebach.

A crucial issue of SK10 is currently ascribed to the input of the WUE estimation (Anderson et al. 2018; Palatella et al. 2014; Sulman et al. 2016). To investigate the sensitivity of the partitioning approach to WUE input, differing T_f were used for the calculation. Figures 4a and 4b show how these modified temperatures and the corresponding WUEs deviated from mean air temperature and WUE_{meanT} (in Fig. 4 we skipped showing results derived with $WUE_{meant-2K}$ and $WUE_{meanT+2K}$ for clarification; corresponding figure including these results can be found in Supplementary material). T_f calculated by considering a logarithmic mean profile implementing MOST varied in the range of mean air temperature ± 2 K (this range of temperature was suggested by Scanlon and Sahu 2008). T_f calculated by means of measured outgoing longwave radiation was mostly higher than mean air temperatures during the day (up to 3 K at forest and 6 K at crop site). The magnitudes of corresponding WUEs decreased/increased (were less/more negative) with higher/lower temperature as stated before. WUE_{MOST} and WUE_{OLR} were within the range of $WUE_{meanT-2K}$ and $WUE_{meanT+2K}$, WUE_{OLR} usually being less negative. Also shown are WUE_{MIN} and WUE_{MAX} not only differing in used temperature, but also in c_i, which represented the outer reasonable margins for WUE input. With $WUE_{MIN,}$ SK10 found valid solutions less often for both study sites – on many days only in the morning or evening hours (see Supplementary material). Also, the morning and evening hours usually produced WUEs of large magnitudes. Figures 4c and 4d show the median of the partitioning fractions for H_2O and CO_2 fluxes in relation to the measured net fluxes (T/ET, NPP/NEE) grouped into classes of 25 W m^{-2} or 5 µmol m^{-2} s^{-1}, respectively, of the total fluxes. With larger measured ET the medians of T/ET increased slightly and converged towards 1. This could be related to the functioning of the method or with the fact that the actual partitioning depends on the total flux magnitude. Such a clear trend was not observed for the medians of NPP/NEE in dependence on the magnitude of NEE. Furthermore, partitioning fractions for H_2O and CO_2 were closer to unity with a less negative WUE. With a

more negative WUE, as e.g. WUE_{MAX}, the medians of the partitioning fractions decreased for H_2O, so estimated T and E converged, and increased for CO_2, such that both R_s and the magnitude of NPP increased. Sulman et al. (2016) have made the same observations. Figures 4e and 4f show all half-hourly partitioning fractions for both scalars as a function of the WUE obtained with the different T_f estimations. While single values scatter widely due to varying factors affecting partitioning in each half-hour, the median over WUE classes of 5 mg g^{-1} including all partitioning approaches revealed a general trend in the partitioning result. With increasing magnitude of WUE the fraction of T in ET decreased, and both CO_2 flux components became larger. For our sites and chosen time periods, the medians of the partitioning fractions ranged between 0.6 and 1 for T/ET, and between 1.1 and 2 for NPP/NEE. Thus, T usually represented the larger fraction of the total water vapor flux. Further, the large range of NPP/NEE indicates a larger impact of uncertain WUE in the CO_2 partitioning than for H_2O, as also reported by Scanlon and Sahu (2008). Furthermore, the differing WUE inputs caused a bigger difference for the cropland than for the forest (Supplementary material). In general, usage of WUE_{MOST} or WUE_{OLR} improved the estimation of R_s compared to the chamber measurements regarding the RMSE and bias (Tab. 1). However, these error quantities were highly sensitive towards outliers.

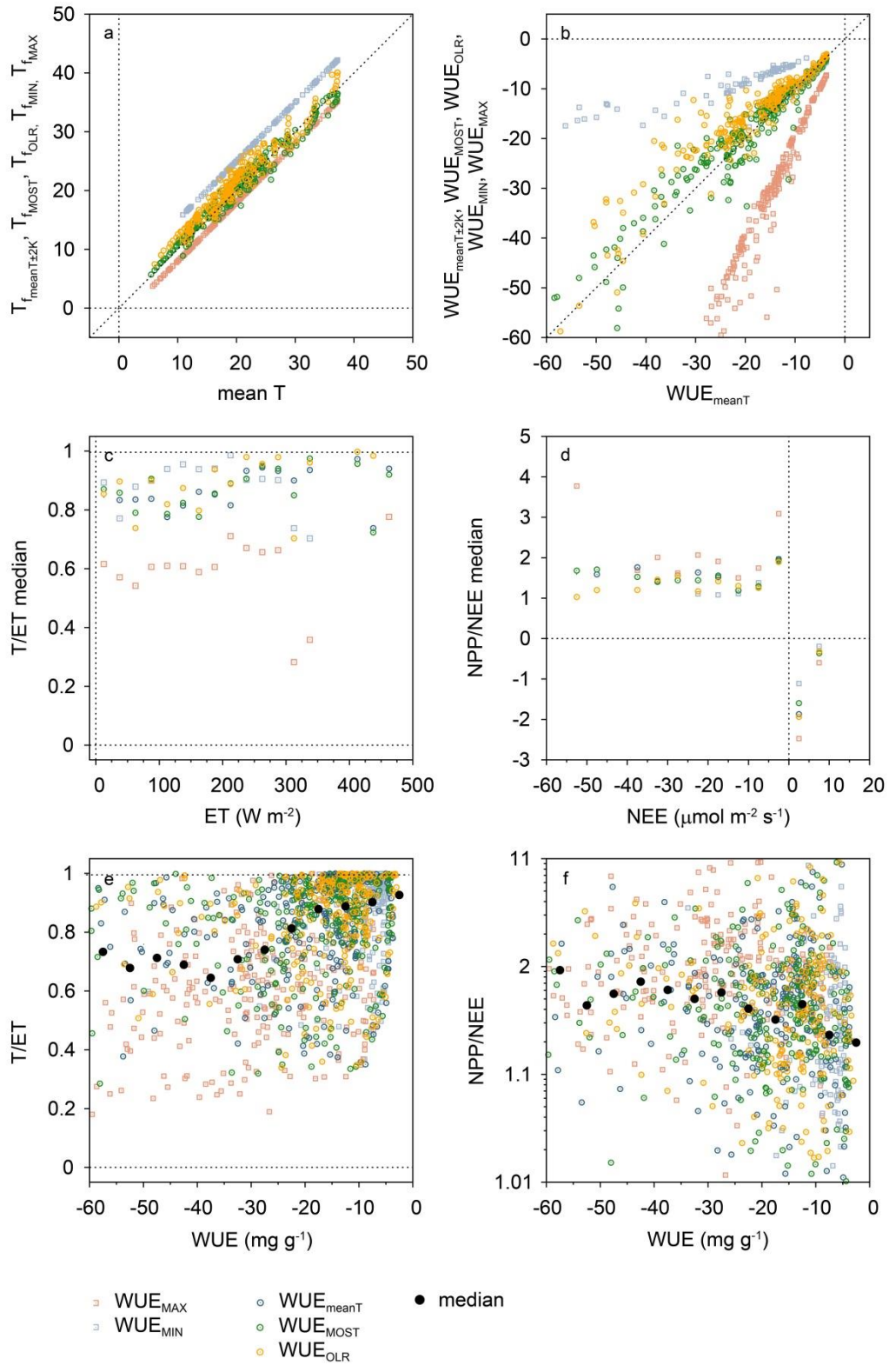

Fig. 4: Comparison of source partitioning results of the approach after Scanlon and Kustas (2010) depending on different water use efficiency (WUE) inputs for both study sites (see Section *Water Use Efficiency* for description; T_f: foliage temperature; ET: evapotranspiration; T: transpiration; NEE: net ecosystem exchange; NPP: net primary production).

3.2 Large Eddy Simulations

The vertical profiles of horizontal wind speed, momentum flux, second-order moments, and vertical wind speed skewness produced by the LES are shown in Figure 5, and they compared qualitatively well with profiles shown by Edburg et al. (2012) and Ouwersloot et al. (2016). Here, no oscillations in the velocity components around the top of the canopy could be observed due to the smooth transition of the PAD at canopy top, as prescribed by Ouwersloot et al. (2016). We also conducted short test runs on the one hand with higher resolution (grid size of 0.05 h_c x 0.05 h_c x 0.05 h_c) and on the other hand with a larger domain size (doubled in x-, y-, and z-direction) to test if our main LES experiments described the turbulence and scalar transport sufficiently, especially near the surface. Even though the costly test runs had a short runtime during which they did not converge, no clear dependence of the domain size could be observed. Small discrepancies between the original LES and the one with higher resolution could be found, where flux profiles adjusted quicker in the latter. The proportion of the resolved scale of the second-order moments was well below 15% in the original LES except in the region below 1.5 h_c. Thus, we assumed that the conducted LES simulated canopy flows and scalar transport reasonably well.

Because the simulated turbulence and the associated calculated fluxes did not show large differences between the two canopy types, only results of the crop canopy are shown in the following (corresponding results of the forest canopy in Supplementary material). Thus, differences in scalar-scalar-correlations and flux profiles between the various cases were caused solely by the differing sink-source-distributions (shape and relative strength of the soil source) and not by differences in the turbulence. Examples of the sampled synthetic high frequency data of *q'* and *c'* are shown in Appendix B for different 'measurement' heights and for the two sink-source-distributions ModelV and ModelB each with the strong soil source (Fig. B.1).

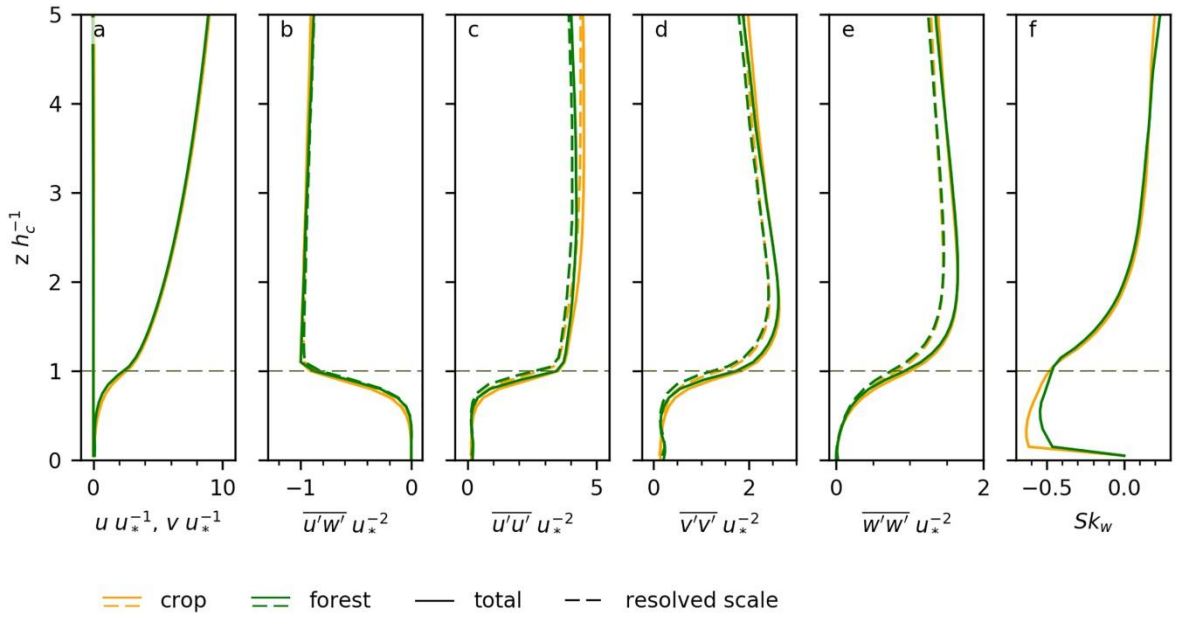

Fig. 5: Mean vertical profiles of streamwise and crosswise velocity (u, v), vertical momentum flux ($\overline{u'w'}$), variances of u, v, and vertical wind velocity (w), and skewness of vertical wind (Sk_w), scaled by friction velocity (u_*) at canopy top. Shown are profiles of the simulations with the crop and forest canopy. The "total" (*non-dashed*) and "resolved scale" (*dashed*) lines differ by the small contribution of small-scale turbulence that cannot be directly simulated by LES and is therefore estimated by its subgrid parametrization (also seen in following figures).

The vertical profiles of the total fluxes of H_2O and CO_2 were very similar and did not show large differences above the canopy between the different sink-source-distributions (ModelV or ModelB) and soil CO_2 source strengths (Fig. 6a, d). The profiles showed differences of typically less than 1% above 1.5 h_c. For CO_2 the varying soil surface sources could be distinguished in the flux profiles of the components originating from the canopy or soil surface (Fig. 6b, c). Vertical profiles of the correlation between *q'* and *c'* showed only larger discrepancies (larger than 1%) between the various experiments up to a measurement height of 3.2 h_c (Fig. 7a). The correlation between fluctuations of H_2O components ($\rho_{q_t'q_e'}$) or of CO_2 components ($\rho_{c_p'c_r'}$) and the transport efficiencies $\rho_{w'q_t'}$ and $\rho_{w'c_p'}$ were dependent on the sink-source-distribution (Fig. 7b, d, e), in which discrepancies vanished above a height of 8 h_c (not shown). The transport efficiencies of the soil sources $\rho_{w'q_e'}$ and $\rho_{w'c_r'}$ were naturally independent of the sink-source-distribution in the canopy and of the source strength. When

comparing $\rho_{w'q_t'}$, $\rho_{w'q_e'}$, $\rho_{w'c_p'}$, and $\rho_{w'c_r'}$ with each other for each sink-source-distribution, differences (larger than 1%) between these transport efficiencies disappeared above 7 h_c.

SK10 was applied to the sampled data at every virtual measurement height. SK10 generally underestimated the magnitudes of CO_2 fluxes originating from the soil surface and the canopy (Fig. 6b, c). Accordingly, the canopy H_2O flux source was underestimated, and the soil source overestimated. Above a height of 1.5 h_c for the low CO_2 soil source and above 2.5 h_c for the strong source, almost no differences between ModelV and ModelB were visible, such that in Figures 6b, 6c, 6e, and 6f data points of ModelV are hidden under data points of ModelB. Above a height of 5 h_c larger discrepancies between the various experiments emerged again (not shown), probably related to the fact that $\rho_{q'c'}$ converged to -1 with increasing height. Below these heights, partitioning results of ModelV converged towards the known input fluxes of the scaled LES. These better results seemed to be connected with the stronger decorrelation between q' and c' observed in the corresponding heights ($|\rho_{q'c'}| < 0.975$; Fig. 7a). Furthermore, the height-dependence of the SK10-estimated flux components was very similar for all four sink-source-distributions (with exception of the lower few h_c of ModelV). Differences between soil source strengths were not detected. However, SK10 produced a difference in the H_2O flux profiles depending on soil source strength, contradicting the differences in the scaling input. This can also be seen in the scatter plots of Figure 8 showing partitioning results for the height of 2.5 h_c. Also, the SK10-based $\rho_{c_p'c_r'}$ and $\sigma_{c_p}^2$ deviated from the known input (Fig. 7b, c, 8d, e). The permitted error between the known $\rho_{q'c'}$ of the synthetic high frequency data and the by SK10 calculated $\rho_{q'c'}$ was set to a maximum of 0.1 (Fig. 7a, 8c).

Up to this point we can conclude that SK10 was not able to infer the correct partitioning, even if the correct leaf-level WUE was used. The magnitude of the difference between WUE_{eco} and canopy-level WUE did not seem to affect the partitioning performance, otherwise both

experiments of ModelV and ModelB with the stronger soil source would have yielded better results than the sink-source-distributions with the lower soil source. A certain degree of decorrelation between *q'* and *c'* is needed for the method to work: $\rho_{q'c'}$ converged slower to -1 with increasing height for ModelV than for ModelB caused by a larger separation of soil source and canopy sink/source. The impact of the WUE input could also have been compensated by the impact of the decorrelation. In the next paragraph we inquire an additional influencing factor for the partitioning performance of SK10.

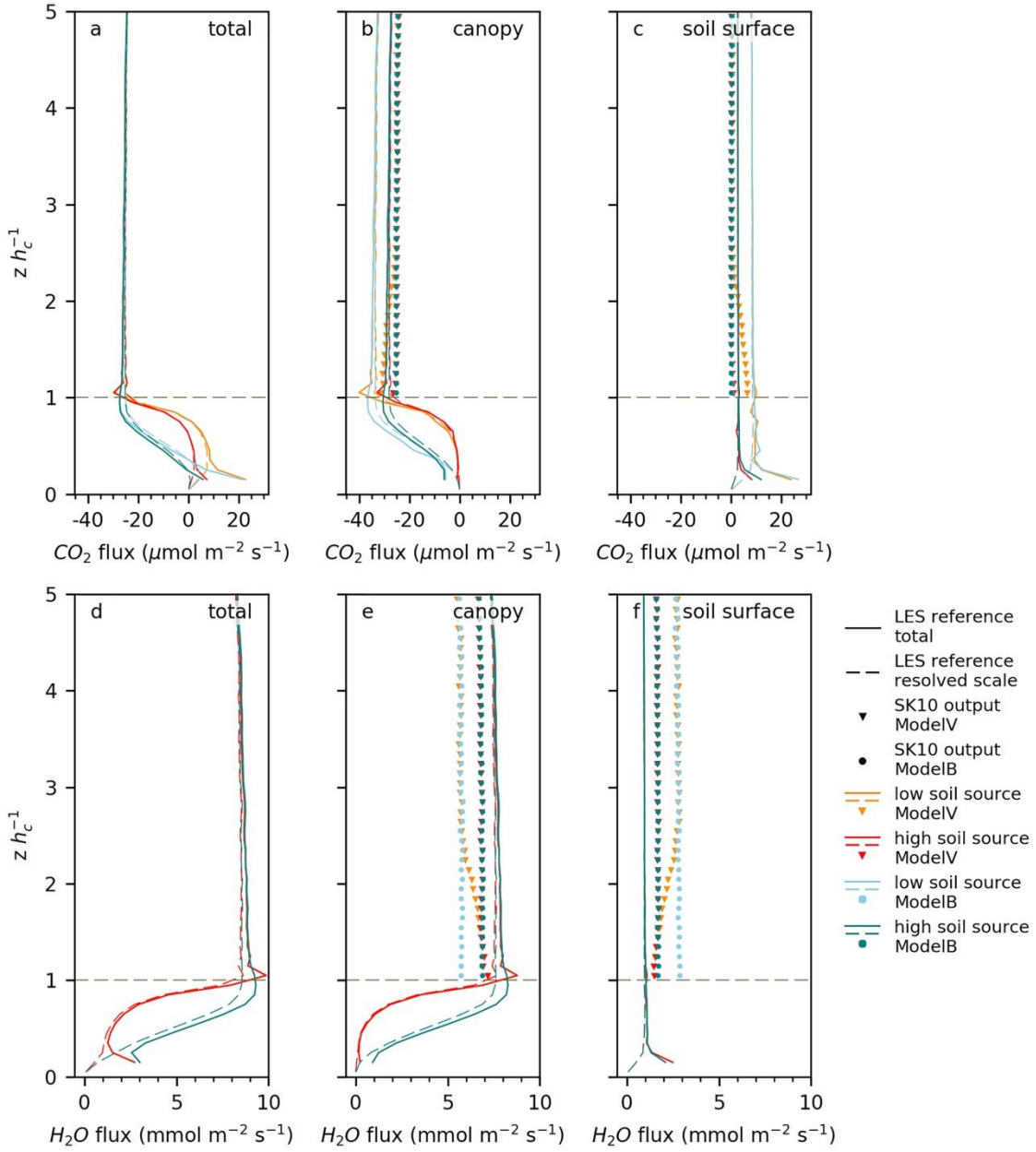

Fig. 6: Vertical profiles of H_2O and CO_2 flux, and their components resulting from LES scaled with the four variations of sink-source-distributions (ModelV or ModelB; low or high soil source) for the crop canopy. For each, the simulations of the resolved (*dashed lines*) and total (resolved + subgrid; *non-dashed lines*) scale are indicated. Also shown are the partitioning results of the approach after Scanlon and Kustas (2010, SK10; *markers*) for each grid height.

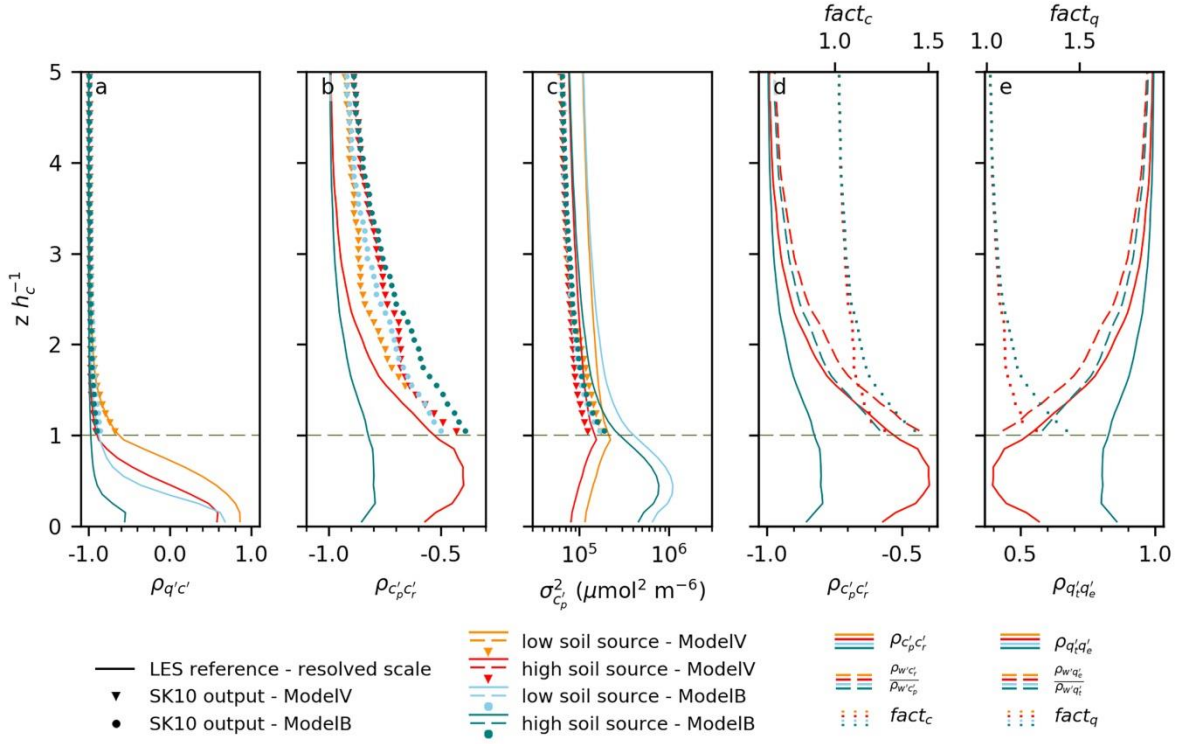

Fig. 7: a)-c) Vertical profiles of $\rho_{q'c'}$, $\rho_{c_p'c_r'}$, and $\sigma_{c_p}{}^2$ resulting from LES scaled with the four variations of sink-source-distributions (ModelV or ModelB; low or high soil source; simulations of the resolved scale; *lines*) for the crop canopy, compared to results of the approach after Scanlon and Kustas (2010, SK10) (*markers*). **d)-e)** Comparison of the two sides of Equations 2 and 3 checking the transfer assumption (*dashed* and *non-dashed lines*) and corresponding correction factors ($fact_q$, $fact_c$, defined in Equation 5 and 6; *dots*).

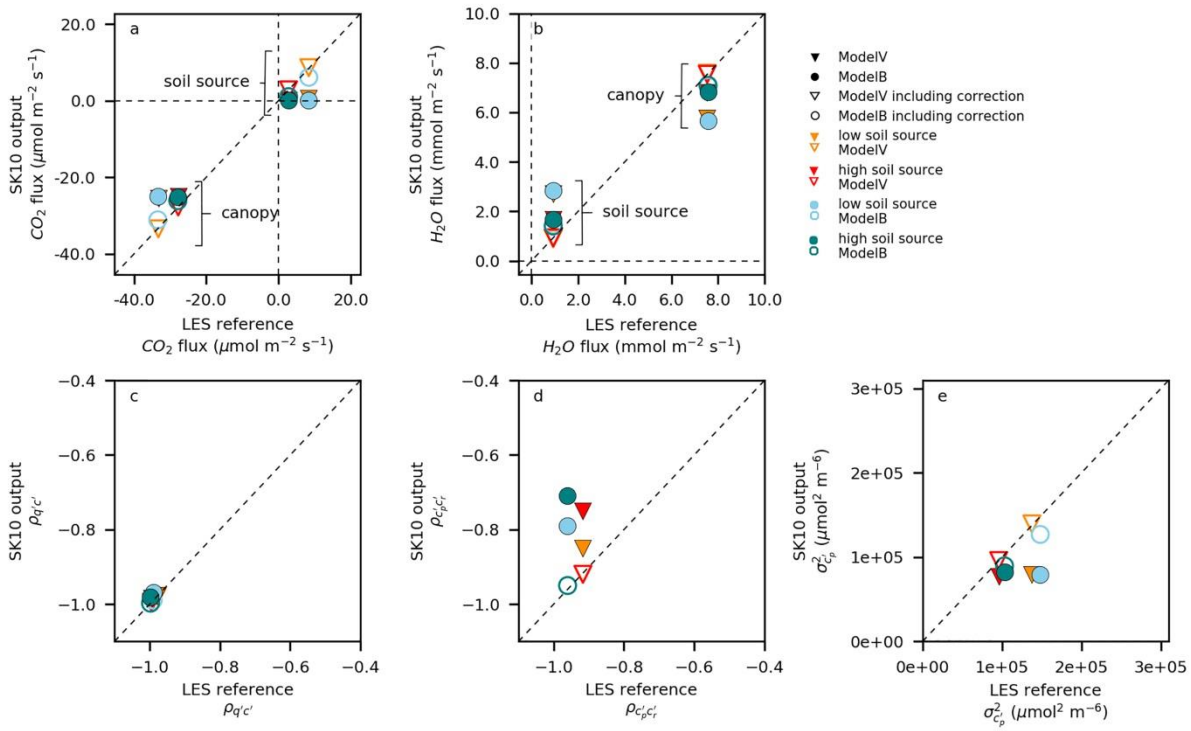

Fig. 8: Comparison of H_2O and CO_2 flux components, $\rho_{q'c'}$, $\rho_{c_p'c_r'}$, and $\sigma_{c_p}^2$ resulting from LES for the four variations of sink-source-distributions (ModelV or ModelB; low or high soil source; simulations of the resolved scale) and the partitioning results of the approach after Scanlon and Kustas (2010, SK10) at a 'measurement' height of 2.5 canopy heights for the crop canopy. Shown are results of the partitioning procedure without (*filled markers*) and with (*non-filled markers*) correction of the transfer assumption.

For the LES analysis, the inaccurate partitioning by SK10 could not be caused by an uncertain WUE input, as was assumed for our field data, because the correct WUE from the scaled LES experiments was used. As seen in Figures 7d and 7e, the approximations made in Equations 2 and 3 (transfer assumption) were invalid for our synthetic experiments, possibly causing the erroneous partitioning results. In the next step, we conducted the source partitioning with SK10 again, including correction factors $fact_q$ and $fact_c$ in Equations 2 and 3, which were known from the scaled LES experiments (Fig. 7d, e).

$$\rho_{q_t'q_e'} = \frac{\rho_{w'q_e'}}{\rho_{w'q_t'}} \cdot fact_q \quad (5)$$

$$\rho_{c_p'c_r'} = \frac{\rho_{w'c_r'}}{\rho_{w'c_p'}} \cdot fact_c \quad (6)$$

Thus, we made sure that the approximations were valid. These correction factors had to be included in the complete system of equations of the SK10 method, because all equations are derived based on these approximations. The relationship between correction factors and partitioning results is non-linear. In this study, the correction factors were between 1.0 and 1.5 decreasing with increasing height, and did only differ between sink-source-distributions (ModelV or ModelB) and not between the low or high soil source (Fig. 7d, e). For ModelB the correction factors had to be larger than for ModelV, which could explain the better results for the latter. Figures 8 and 9 show updated source partitioning results by SK10 including these correction factors. In this case, SK10 almost perfectly matched the known input of the scaled LES experiments. Small discrepancies were observed above a height of 2 h_c especially for ModelB. For the forest-like canopy, the correction of the transfer assumption brought perfect partitioning results up to a height of 4 h_c (Supplementary material). This was due to the fact that the necessary decorrelation between q' and c' reached higher in the simulation with the forest canopy than with the crop canopy.

To transfer these results from the LES experiments to study sites, the SK10 method would benefit from an EC measurement height in the lower roughness sublayer to ensure a certain degree of decorrelation of the scalars (which is not a measurement height usually chosen for high-quality net flux measurements). At the same time, however, a larger measurement height would ensure more likely the validity of the transfer assumption. A comparison of Figures 6, 7d, and 7e indicates that the latter factor compensates the former to some degree, such that without known correction factors for the transfer assumption, no measurement height is ideal. However, the better performance of ModelV close to the canopy in Figure 6 indicates that the net effect of both factors leads to better results with measurements low above the canopy.

To further investigate the influence of the turbulence and the canopy on the partitioning performance, additional LES runs with e.g., larger LAI would be necessary. With changed turbulence the transport efficiencies and scalar-scalar-correlations would differ. Huang et al. (2013) stated that the correlation between *q'* and *c'* increased with increasing canopy density in their LES studies. LAI might therefore have a similarly ambiguous effect on SK10's performance as measurement height. This conundrum could only be solved if a way was found to estimate correction factors for $\rho_{c_p'c_r'}$ and $\rho_{q_t'q_e'}$ in field studies.

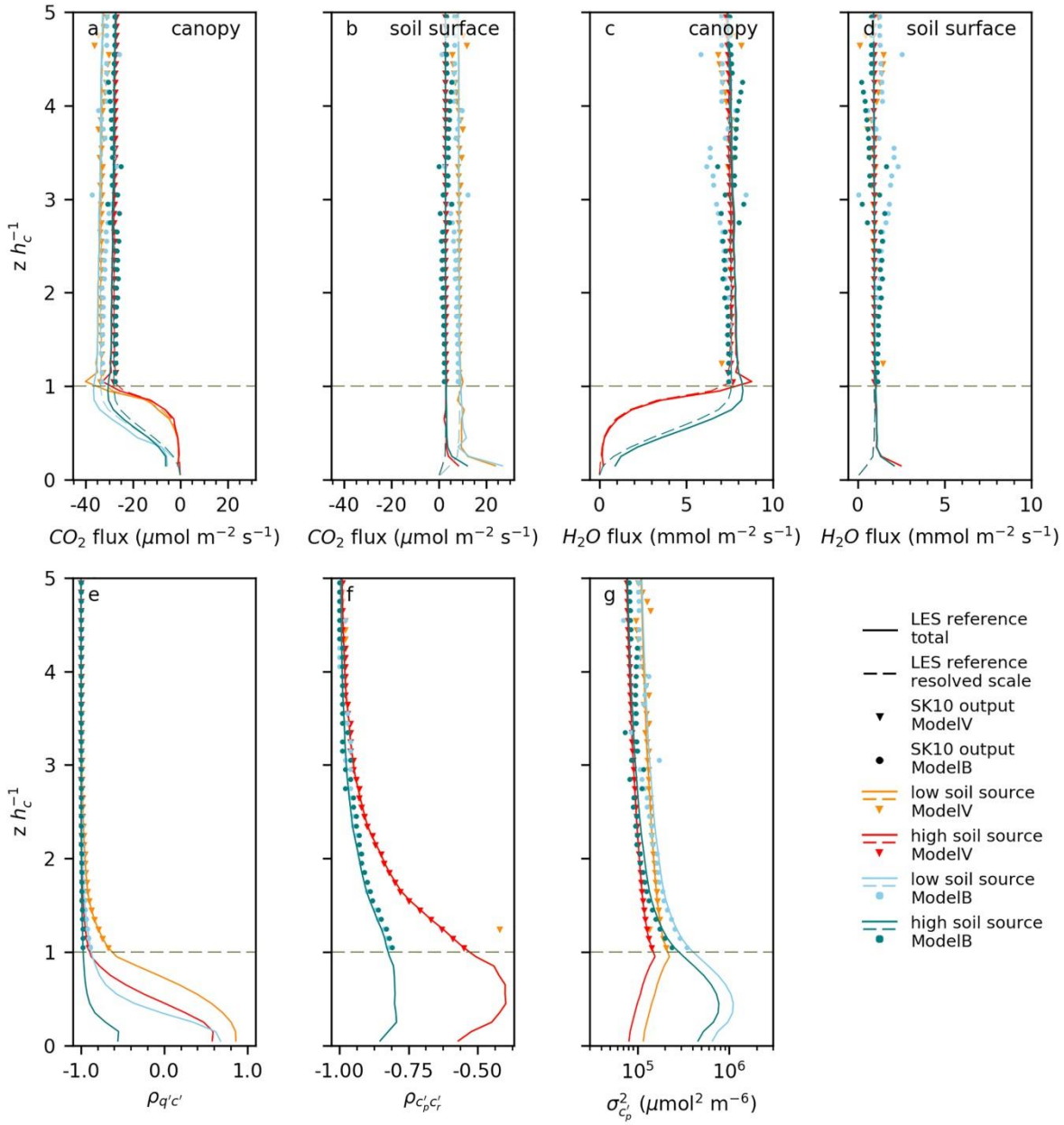

Fig. 9: Vertical profiles of H_2O and CO_2 flux components, $\rho_{q'c'}$, $\rho_{c_p'c_r'}$, and $\sigma_{c_p'}^2$ resulting from LES scaled with the four variations of sink-source-distributions (ModelV or ModelB; low or high soil source) for the crop canopy. For the flux components, the simulations of the resolved (*dashed lines*) and total (resolved + subgrid; *non-dashed lines*) scale are indicated. Also, the partitioning results of the approach after Scanlon and Kustas (2010, SK10; *markers*) including the correction of the transfer assumption are shown for each grid height.

At our cropland and forest study sites, WUE inputs varied between one third of and three times of WUE_{meanT} depending on the calculation of T_f and the magnitude of c_i (Fig. 4). In order to put the sensitivity to WUE input in context to the possible error in the transfer assumption discussed above, we repeated the SK10-based analysis of the LES data with corrected transfer assumption and with the variability of WUE input as seen in the field data analysis. However, no valid solutions could be found by the algorithm below a height of 4 h_c. Instead, WUE input could only be changed by up to minus 90% or plus 24% while still obtaining partitioning solutions for heights of interest (below 4 h_c). In Figure 10 partitioning fractions of the H_2O and CO_2 fluxes are shown as a function of WUE input for each sink-source-distribution at a virtual measurement height of 2.5 h_c. Other than at our study sites (Fig. 4e, f), in this case the true WUE and partitioning fractions were known. The transfer assumption was applied in its original form (Eqs. 2, 3; filled markers in Fig. 10) and with correction factors (Eqs. 5, 6; non-filled markers), such that the combined effect of both sources of error (wrong WUE input and invalid transfer assumption) on the partitioning result could be seen (also see Fig. B.2 in Appendix B). Both sink-source-distributions, ModelV and ModelB, show the same trends in the relation of T/ET and NPP/NEE with WUE. With the correct WUE and including the correction factors, small discrepancies between true and estimated partitioning factors were observed for ModelB, as described above (Fig. 8, 9). For H_2O, the range of T/ET for varying WUEs was smaller with a corrected transfer assumption than without. Thus, the potential error made with wrong WUE inputs was smaller. An overestimation of the magnitude of WUE (more negative) led to an overestimation of T with

841 corrected, and an underestimation with uncorrected transfer assumption. Figure 10 also
842 indicates that without correction of the transfer assumption, typically a slightly
843 underestimated magnitude of WUE will lead to a partitioning fraction close to the truth. For
844 CO_2, the variability in NPP/NEE was larger for the applications with corrected transfer
845 assumption than without (note the logarithmic y-axes), which is contrary to the behavior of
846 T/ET. NPP/NEE was very small with the incorrect transfer assumption. At our study sites we
847 often observed an overestimation of the CO_2 components (Fig. 3). In contrast, in the LES-
848 based analysis NPP/NEE was underestimated without correction factors, even with the correct
849 WUE. With a correct WUE input the errors made by an invalid transfer assumption were
850 mostly smaller for the low soil source than for the high soil source.
851 Considering the medians in Figure 4e and 4f, E, R_s, and |NPP| increased and T decreased by
852 increasing the magnitude of WUE (more negative) at our study sites, thus, describing a
853 similar behavior as the partitioning factors derived by SK10 with an incorrect transfer
854 assumption in the LES-based analysis. But the range of the varying WUE was larger at our
855 study sites than the possible range in the LES-based analysis, and at the study sites differing
856 WUEs of multiple half-hours on various days with varying weather conditions and different
857 canopies were compared.
858 Sulman et al. (2016) reported a higher sensitivity of E and R_s to the WUE input than of T and
859 NPP. By varying WUE, the absolute change of stomatal and non-stomatal processes of H_2O
860 or CO_2 were identical, because they were summing up to the unchanged, measured net fluxes.
861 But the relative change differed because of the much smaller magnitude of non-stomatal
862 processes than of stomatal processes (Sulman et al. 2016). We also observed that the differing
863 input of WUE had a larger relative effect on soil source fluxes than on fluxes originating from
864 the canopy (relative residuals in Fig. B.2). The errors in the final flux partitioning obtained

when not using the true known WUE input, were on the same order of magnitude as those obtained when ignoring the correction of the transfer assumption (Fig. 10).

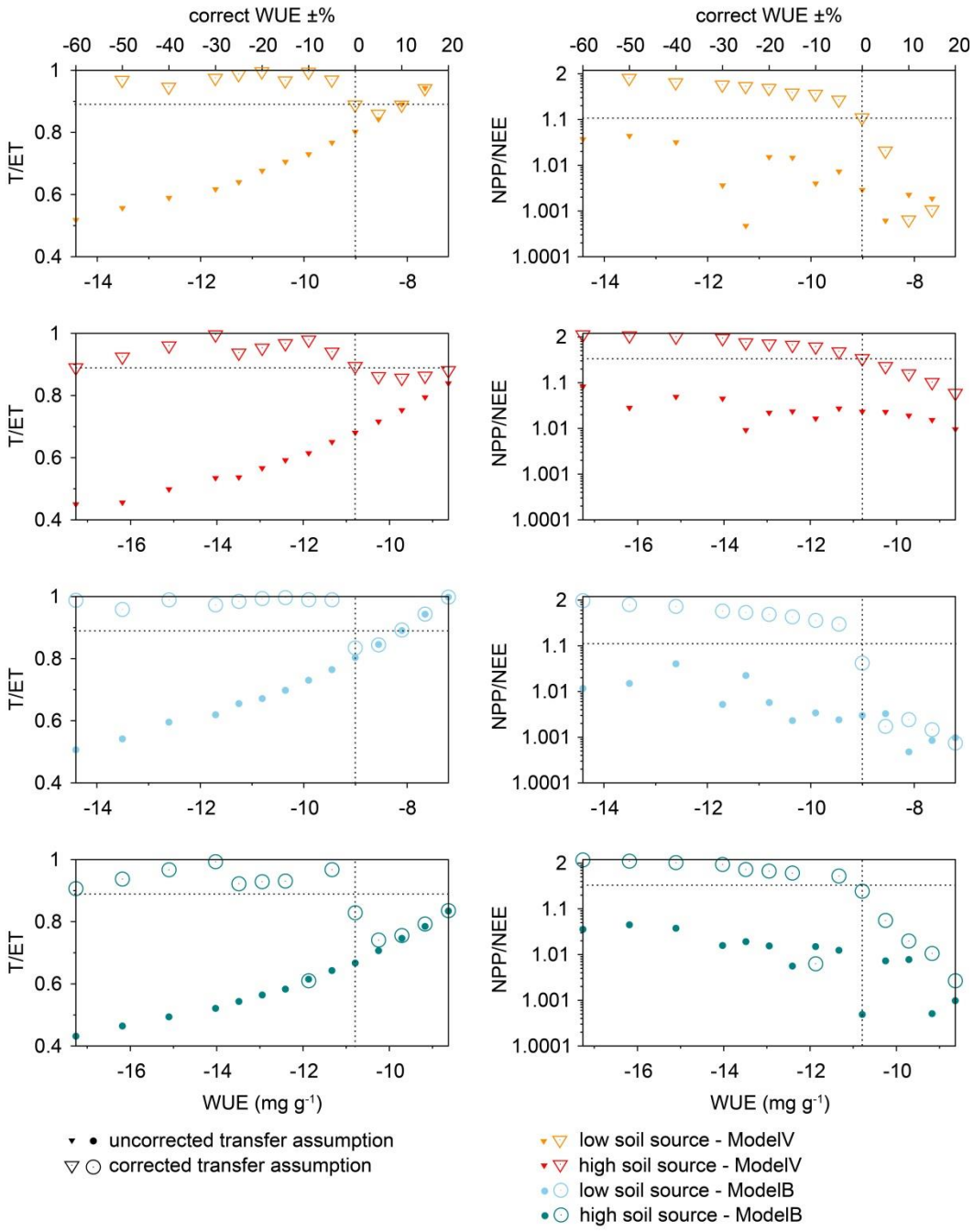

Fig. 10: Results of partitioning fractions for H_2O (T/ET, *left*) and CO_2 (NPP/NEE, *right*) fluxes in relation to the input water use efficiency (WUE). The source partitioning approach after Scanlon and Kustas (2010) was applied to synthetic high frequency data from LES scaled with the four variations of sink-source-distributions (ModelV or ModelB; low or high soil source) at a 'measurement' height of 2.5 canopy heights for the crop canopy with corrected (*non-filled markers*) and uncorrected (*filled markers*) transfer assumption. The true known partitioning factors and WUE input are indicated by the *dashed lines*.

The LES-based analysis provided some insights for understanding the presented field results, interpreting past and future results from the application of SK10 to field data, and possible future efforts to improve the method. Clearly, a correct WUE estimate is favorable (condition a), as has already been mentioned by Anderson et al. (2018) and Sulman et al. (2016). However, even a correct WUE can yield erroneous partitioning results, if the relations of transport efficiencies of the scalars deviate too much from the current method assumption (condition b). Unfortunately, whereas we could deduce the correction factors for this deviation in the LES study, there is currently no way to derive these factors from field data. More research is required to establish their dependence on canopy geometry, turbulence conditions, and vertical source distribution. Finally (condition c), a minimum decorrelation between q' and c' is required to ensure that the solution is robust, i.e. the results are not strongly dependent on small uncertainties in other input variables. With measurement height closer to the canopy, decorrelation between H_2O and CO_2 fluctuations increase. However, at the same time the transfer assumption is less likely to be valid (Fig. 7d, e). Therefore, an optimum measurement height near the canopy top may exist for applications of SK10, being a tradeoff between optimal decorrelation and optimal validity of the transfer assumption. For future improvements of the method itself, or for an associated quality-flagging detecting unfavorable situations, the effect of each of the conditions a, b, or c could be quantified in situations where the remaining two conditions are met, through the process of exclusion. For example, long time series with precise in-situ measurements of leaf-level WUE, filtered for a sufficient decorrelation of q' and c', may help frame the magnitude of the effect of the transfer assumption even in the field. Alternatively and with a potentially higher precision, tracer experiments might enable direct measurements of the transport efficiencies of scalar flux components in the field. Such results would be particularly helpful to resolve the

conundrum that in our study, SK10 tended to overestimate soil fluxes in the field but underestimate them in the LES-based analysis.

4. Summary and Conclusions

In this study, we applied the source partitioning method SK10 to data of our study sites and analyzed how the partitioning results depend on the WUE input. Compared to R_s chamber measurements and to E_{soil} calculated based on Beer's law depending on LAI, the partitioning results for the forest site in Wüstebach were more satisfying than for the cropland in Selhausen for the respective study periods. The partitioning method's performance was sensitive to precipitation events and to the maturity of the crop, connected to the photosynthetic activity and the relation between stomatal and non-stomatal processes in the crop canopy. With a less active canopy, relative stronger soil sources, or with a higher distance between canopy and soil sink/sources, SK10 performed better at our study sites. The estimation of WUE input based on T_f derived with measurements of outgoing longwave radiation (WUE_{OLR}) or by considering a logarithmic mean profile implementing MOST (WUE_{MOST}) improved the partitioning performance compared to R_s measurements. Inclusion of direct measurements of WUE on leaf-level would improve the method's performance (Anderson et al. 2018; Sulman et al. 2016), but such measurements are not available at most study sites. An intermediate improvement could be to estimate the leaf-internal CO_2 concentration rather than assuming a constant value. Parameterizations for c_i have been developed in the context of models for stomatal conductance (Ronda et al. 2001) and applied to the SK10 method by van de Boer (2015).

In a next step, we applied SK10 to synthetic high frequency data generated by LES and analyzed the partitioning performance depending on canopy type, measurement height, and given sink-source-distributions. Primarily, approximations involved in SK10 (Eqs. 2, 3; transfer assumption) were checked in the LES. Furthermore, for the synthetic data the dependence of the partitioning result to WUE input was analyzed as well. Because simulated turbulence did not differ much between PAD types, also SK10's performance did not differ

significantly. The performance was sensitive to the virtual ‘measurement’ height and to the corresponding decorrelation between q' and c'. The decorrelation above the canopy was stronger and reached higher for the forest canopy, for the v-shaped sink-source-distribution (and thus for a higher separation between soil sources and canopy sink/source), and/or for the distributions with low soil sources. To further investigate the influence of the canopy architecture and resulting turbulence on the partitioning performance, additional LES runs with e.g., larger LAI would be necessary. Similar behavior of SK10’s performance depending on differing input of WUE could be reproduced with the synthetic experiments as observed at the study sites. Primarily, our LES study indicated that next to a precise WUE estimation, the validity of the transfer assumption was a crucial point for a correct application of SK10. Therefore, further work would be necessary for a thorough assessment of the conditions at study sites affecting the validity of the transfer assumption. These conditions could include measurement height above the canopy, separation between soil sources and canopy sink/source, and the corresponding transport efficiencies.

Acknowledgements

This research was supported by the German Federal Ministry of Education and Research BMBF, project IDAS-GHG [grant number 01LN1313A]. The measurement infrastructure providing observational data was supported by the German Research Foundation DFG through the Transregional Collaborative Research Centre 32 (TR 32) and Terrestrial Environmental Observatories (TERENO). The computational facilities have been provided by the Netherlands Science Foundation under contract NWO 15774 [grant number SH-312-15]. The authors thank all technicians, engineers, and laboratory assistances in TR32 and TERENO for providing measurements of the test sites. Finally, we thank the reviewer for their helpful comments that improved the quality of this manuscript.

References

Anderson, R.G., Zhang, X., Skaggs, T.H., 2018. Measurement and partitioning of evapotranspiration for application to vadose zone studies. Vadose Zone J. 16 (13), 1-9, https://doi.org/10.2136/vzj2017.08.0155.

Bink, N.J., Meesters, A.G.C.A., 1997. Comment on 'Estimation of surface heat and momentum fluxes using the flux-variance method above uniform and non-uniform terrain' by Katul et al. (1995). Boundary-Layer Meteorol. 84 (3), 497-502, https://doi.org/10.1023/A:1000427431944.

Bogena, H.R., Bol, R., Borchard, N., Brüggemann, N., Diekkrüger, B., Drüe, C., Groh, J., Gottselig, N., Huisman, J.A., Lücke, A., Missong, A., Neuwirth, B., Pütz, T., Schmidt, M., Stockinger, M., Tappe, W., Weihermüller, L., Wiekenkamp, I., Vereecken, H., 2015. A terrestrial observatory approach to the integrated investigation of the effects of deforestation on water, energy, and matter fluxes. Science China: Earth Sciences 58 (1), 6175, https://doi.org/10.1007/s11430-014-4911-7.

Campbell, G.S., Norman, J.M., 1998. An introduction to environmental biophysics. Springer, New York, pp. 286.

Cassiani, M., Katul, G.G., Albertson, J.D., 2008. The effects of canopy leaf area index on airflow across forest edges: large-eddy simulation and analytical results. Boundary-Layer Meteorol. 126 (3), 433-460, https://doi.org/10.1007/s10546-007-9242-1.

Chen, J.M., 1996. Optically-based methods for measuring seasonal variation of leaf area index in boreal conifer stands. Agric. For. Meteorol. 80 (2-4), 135-163, https://doi.org/10.1016/0168-1923(95)02291-0.

Denmead, O.T., Dunin, F.X., Leuning, R., Raupach, M.R., 1996. Measuring and modelling soil evaporation in wheat crops. Phys. Chem. Earth 21 (3), 97-100, https://doi.org/10.1016/S0079-1946(97)85567-X.

Detto, M., Katul, G.G., 2007. Simplified expressions for adjusting higher-order turbulent statistics obtained from open path gas analyzers. Boundary-Layer Meteorol. 122 (1), 205-216, https://doi.org/10.1007/s10546-006-9105-1.

Dupont, S., Brunet, Y., 2008. Influence of foliar density profile on canopy flow: a large-eddy simulation study. Agric. For. Meteorol. 148 (6-7), 976-990, https://doi.org/10.1016/j.agrformet.2008.01.014.

Edburg, S.L., Stock, D., Lamb, B.K., Patton, E.G., 2012. The effect of the vertical source distribution on scalar statistics within and above a forest canopy. Boundary-Layer Meteorol. 142 (3), 365-382, https://doi.org/10.1007/s10546-011-9686-1.

Finnigan, J.J., Shaw, R.H., Patton, E.G., 2009. Turbulence structure above a vegetation canopy. J. Fluid Mech. 637, 387-424, https://doi.org/10.1017/S0022112009990589.

Good, S.P., Soderberg, K., Guan, K., King, E.G., Scanlon, T.M., Caylor, K.K., 2014. δ^2H isotopic flux partitioning of evapotranspiration over a grass field following a water pulse and subsequent dry down. Water Resour. Res. 50 (2), 1410-1432, https://doi.org/10.1002/2013WR014333.

Graf, A., Herbst, M., Weihermüller, L., Huisman, J.A., Prolingheuer, N., Bornemann, L., Vereecken, H., 2012. Analyzing spatiotemporal variability of heterotrophic soil

993 respiration at the field scale using orthogonal functions. Geoderma 181, 91-101,
994 https://doi.org/10.1016/j.geoderma.2012.02.016.
995 Graf, A., Bogena, H.R., Drüe, C., Hardelauf, H., Pütz, T., Heinemann, G., Vereecken, H.,
996 2014. Spatiotemporal relations between water budget components and soil water content
997 in a forested tributary catchment. Water Resour. Res. 50 (6), 4837-4857,
998 https://doi.org/10.1002/2013WR014516.
999 Gspaltl, M., Bauerle, W., Binkley, D., Sterba, H., 2013. Leaf area and light use efficiency
1000 patterns of Norway spruce under different thinning regimes and age classes. Forest Ecol.
1001 Manag. 288, 49-59, https://doi.org/10.1016/j.foreco.2011.11.044.
1002 Heus, T., van Heerwaarden, C.C., Jonker, H.J.J., Pier Siebesma, A., Axelsen, S., van den
1003 Dries, K., Geoffroy, O., Moene, A.F., de Roode, S.R., Vilà-Guerau de Arellano, J., 2010.
1004 Formulation of the Dutch Atmospheric Large-Eddy Simulation (DALES) and overview
1005 of its applications. Geosci. Model Dev. 3 (2), 415-444, https://doi.org/10.5194/gmd-
1006 3-415-2010.
1007 Hill, R.J., 1989. Implications of Monin-Obukhov Similarity Theory for scalar quantities. J.
1008 Atmos. Sci. 46 (14), 2236-2244.
1009 Huang, J., Katul, G., Albertson, J., 2013. The role of coherent turbulent structures in
1010 explaining scalar dissimilarity within the canopy sublayer. Environ. Fluid Mech. 13 (6),
1011 571-599, https://doi.org/10.1007/s10652-013-9280-9.
1012 I.U.S.S. Working Group, 2006. World reference base for soil resources 2006. A framework
1013 for international classification, correlation and communication. In: World Soil Resources
1014 Reports No. 103. FAO, Rome, pp. 128.
1015 Katul, G., Goltz, S.M., Hsieh, C., Cheng, Y., Mowry, F., Sigmon, J., 1995. Estimation of
1016 surface heat and momentum fluxes using the flux-variance method above uniform and
1017 non-uniform terrain. Boundary-Layer Meteorol. 74 (3), 237-260,
1018 https://doi.org/10.1007/BF00712120.
1019 Kool, D., Agam, N., Lazarovitch, N., Heitmann, J.L., Sauer, T.J., Ben-Gal, A., 2014. A
1020 review of approaches for evapotranspiration partitioning. Agric. For. Meteorol. 184,
1021 56-70, https://doi.org/10.1016/j.agrformet.2013.09.003.
1022 Kormann, R., Meixner, F.X., 2001. An analytical footprint model for non-neutral
1023 stratification. Boundary-Layer Meteorol. 99 (2), 207-224,
1024 https://doi.org/10.1023/A:1018991015119.
1025 Lamaud, E., Irvine, M., 2006. Temperature-humidity dissimilarity and heat-to-water-vapour
1026 transport efficiency above and within a pine forest canopy: the role of the Bowen ratio.
1027 Boundary-Layer Meteorol. 120 (1), 87-109, https://doi.org/10.1007/s10546-005-9032-6.
1028 Lasslop, G., Reichstein, M., Papale, D., Richardson, A.D., Arneth, A., Barr, A., Stoy, P.,
1029 Wohlfahrt, G., 2010. Separation of net ecosystem exchange into assimilation and
1030 respiration using a light response curve approach: critical issues and global evaluation.
1031 Global Change Biol. 16 (1), 187-208, https://doi.org/10.1111/j.1365-2486.2009.02041.x.
1032 Mauder, M., Cuntz, M., Drüe, C., Graf, A., Rebmann, C., Schmid, H.P., Schmidt, M.,
1033 Steinbrecher, R., 2013. A strategy for quality and uncertainty assessment of long-term
1034 eddy-covariance measurements. Agric. For. Meteorol. 169, 122-135,
1035 https://doi.org/10.1016/j.agrformet.2012.09.006.

Moene, A.F., Schüttemeyer, D., 2008. The effect of surface heterogeneity on the temperature-humidity correlation and the relative transport efficiency. Boundary-Layer Meteorol. 129, 99-113, https://doi.org/10.1007/s10546-008-9312-z.

Ney, P., Graf, A., 2018. High-resolution vertical profile measurements for carbon dioxide and water vapour concentrations within and above crop canopies. Boundary-Layer Meteorol. 166, 449-473, https://doi.org/10.1007/s10546-017-0316-4.

Ney, P., Schmidt, M., Klosterhalfen, A., Graf, A., 2017. A high-resolution measurement technique for vertical CO_2 and H_2O profiles within and above crop canopies and its use for flux partitioning. Poster presentation, EGU General Assembly 2017, Vienna, Austria, 23-28 Apr 2017.

Ney, P., Graf, A., Bogena, H., Diekkrüger, B., Drüe, C., Esser, O., Heinemann, G., Klosterhalfen, A., Pick, K., Pütz, T., Schmidt, M., Valler, V., Vereecken, H., unpublished data. CO_2 fluxes before and after partially deforestation of a Central European spruce forest. Agric. For. Meteorol.

Ouwersloot, H.G., Moene, A.F., Attema, J.J., Vilà-Guerau de Arellano, J., 2016. Large-Eddy Simulation comparison of neutral flow over a canopy: sensitivities to physical and numerical conditions, and similarity to other representations. Boundary-Layer Meteorol. 162 (1), 71-89, https://doi.org/10.1007/s10546-016-0182-5.

Palatella, L., Rana, G., Vitale, D., 2014. Towards a flux-partitioning procedure based on the direct use of high-frequency eddy-covariance data. Boundary-Layer Meteorol. 153 (2), 327-337, https://doi.org/10.1007/s10546-014-9947-x.

Reichstein, M., Falge, E., Baldocchi, D., Papale, D., Aubinet, M., Berbigier, P., Bernhofer, C., Buchmann, N., Gilmanov, T., Granier, A., Grünwald, T., Havránková, K., Ilvesniemi, H., Janous, D., Knohl, A., Laurila, T., Lohila, A., Loustau, D., Matteucci, G., Meyers, T., Miglietta, F., Ourcival, J.-M., Pumpanen, J., Rambal, S., Rotenberg, E., Sanz, M., Tenhunen, J., Seufert, G., Vaccari, F., Vesala, T., Yakir, D., Valentini, R., 2005. On the separation of net ecosystem exchange into assimilation and ecosystem respiration: review and improved algorithm. Global Change Biol. 11 (9), 1424-1439, https://doi.org/10.1111/j.1365-2486.2005.001002.x.

Reichstein, M., Stoy, P.C., Desai, A.R., Lasslop, G., Richardson, A.D., 2012. Partitioning of net fluxes. In: Aubinet, M., Vesala, T., Papale, D. (Eds.), Eddy covariance. A practical guide to measurement and data analysis. Springer, Dordrecht, Heidelberg, London, New York, pp. 263-289.

Ronda, R.J., de Bruin, H.A.R., Holtslag, A.A.M., 2001. Representation of the canopy conductance in modeling the surface energy budget for low vegetation. J. Appl. Meteorol. Climatol. 40 (8), 1431-1444, https://doi.org/10.1175/1520-0450(2001)040<1431:ROTCCI>2.0.CO;2.

Scanlon, T.M., Albertson, J.D., 2001. Turbulent transport of carbon dioxide and water vapor within a vegetation canopy during unstable conditions: identification of episodes using wavelet analysis. J. Geophys. Res. 106 (D7), 7251-7262, https://doi.org/10.1029/2000JD900662.

Scanlon, T.M., Kustas, W.P., 2010. Partitioning carbon dioxide and water vapor fluxes using correlation analysis. Agric. For. Meteorol. 150 (1), 89-99, https://doi.org/10.1016/j.agrformet.2009.09.005.

Scanlon, T.M., Kustas, W.P., 2012. Partitioning evapotranspiration using an eddy covariance-based technique: improved assessment of soil moisture and land-atmosphere exchange dynamics. Vadose Zone J. 11 (3), https://doi.org/10.2136/vzj2012.0025.

Scanlon, T.M., Sahu, P., 2008. On the correlation structure of water vapor and carbon dioxide in the atmospheric surface layer: a basis for flux partitioning. Water Resour. Res. 44 (10), W10418, pp. 15, https://doi.org/10.1029/2008WR006932.

Sellers, P.J., Berry, J.A., Collatz, G.J., Field, C.B., Hall, F.G., 1992. Canopy reflectance, photosynthesis, and transpiration. III. A reanalysis using improved leaf models and a new canopy integration scheme. Remote Sens. Environ. 42 (3), 187-216, https://doi.org/10.1016/0034-4257(92)90102-P.

Skaggs, T.H., Anderson, R.G., Alfieri, J.G., Scanlon, T.M., Kustas, W.P., 2018. Fluxpart: Open source software for partitioning carbon dioxide and water vapor fluxes. Agric. For. Meteorol. 253-254, 218-224, https://doi.org/10.1016/j.agrformet.2018.02.019.

Špunda, V., Kalina, J., Urban, O., Luis, V.C., Sibisse, I., Puértolas, J., Šprtová, M., Marek, M.V., 2005. Diurnal dynamics of photosynthetic parameters of Norway spruce trees cultivated under ambient and elevated CO_2: the reasons of midday depression in CO_2 assimilation. Plant Sci. 168 (5), 1371-1381, https://doi.org/10.1016/j.plantsci.2005.02.002.

Stoy, P.C., Katul, G.G., Siqueira, M.B.S., Juang, J.-Y., Novick, K.A., McCarthy, H.R., Oishi, C., Uebelherr, J.M., Kim, H.S., Oren, R., 2006a. Separating the effects of climate and vegetation on evapotranspiration along a successional chronosequence in the southeastern US. Global Change Biol. 12 (11), 2115-2135, https://doi.org/10.1111/j.1365-2486.2006.01244.x.

Stoy, P.C., Katul, G.G., Siqueira, M.B.S., Juang, J.-Y., Novick, K.A., Uebelherr, J.M., Oren, R., 2006b. An evaluation of models for partitioning eddy covariance-measured net ecosystem exchange into photosynthesis and respiration. Agric. For. Meteorol. 141 (1), 2-18, https://doi.org/10.1016/j.agrformet.2006.09.001.

Sulman, B.N., Roman, D.T., Scanlon, T.M., Wang, L., Novick, K.A., 2016. Comparing methods for partitioning a decade of carbon dioxide and water vapor fluxes in a temperate forest. Agric. For. Meteorol. 226-227, 229-245, https://doi.org/10.1016/j.agrformet.2016.06.002.

van de Boer, A., 2015. Atmospheric turbulence over crops. Confronting theories with observations. PhD thesis, Wageningen University, Wageningen, NL.

Wang, W., Smith, J.A., Ramamurthy, P., Baeck, M.L., Bou-Zeid, E., Scanlon, T., 2016. On the correlation of water vapor and CO_2: application to flux partitioning of evapotranspiration. Water Resour. Res. 52 (12), 9452-9469, https://doi.org/10.1002/2015WR018161.

Weihermüller, L., Huisman, J.A., Lambot, S., Herbst, M., Vereecken, H., 2007. Mapping the spatial variation of soil water content at the field scale with different ground penetrating radar techniques. J. Hydrol. 340 (3-4), 205-216, https://doi.org/10.1016/j.jhydrol.2007.03.013.

Weiskittel, A.R., Kershaw Jr., J.A., Hofmeyer, P.V., Seymour, R.S., 2009. Species differences in total and vertical distribution of branch- and tree-level leaf area for the five

primary conifer species in Maine, USA. Forest Ecol. Manag. 258 (7), 1695-1703, https://doi.org/10.1016/j.foreco.2009.07.035.
Williams, M., Rastetter, E.B., Fernandes, D.N. Goulden, M.L., Wofsy, S.C., Shaver, G.R., Melillo, J.M., Munger, J.W., Fan, S.-M., Nadelhoffer, K.J., 1996. Modelling the soil-plant-atmosphere continuum in a Quercus-Acer stand at Harvard Forest: the regulation of stomatal conductance by light, nitrogen and soil/plant hydraulic properties. Plant Cell Environ. 19 (8), 911-927, https://doi.org/10.1111/j.1365-3040.1996.tb00456.x.
Williams, C.A., Scanlon, T.M., Albertson, J.D., 2007. Influence of surface heterogeneity on scalar dissimilarity in the roughness sublayer. Boundary-Layer Meteorol. 122 (1), 149-165, https://doi.org/10.1007/s10546-006-9097-x.
Xue, Q., Weiss, A., Arkebauer, T.J., Baenziger, P.S., 2004. Influence of soil water status and atmospheric vapor pressure deficit on leaf gas exchange in field-grown winter wheat. Environ. Exp. Bot. 51 (2), 167-179, https://doi.org/10.1016/j.envexpbot.2003.09.003.

APPENDIX

A. Source Partitioning Based on High Frequency Data

Scanlon and Sahu (2008) and Scanlon and Kustas (2010) provided a system of equations for the source partitioning of H_2O and CO_2 fluxes including following essential equation, which was further modified and reported by Palatella et al. (2014, Equation 29, page 331) as follows:

$$\mathrm{WUE} = \frac{\overline{w'c'}}{\overline{w'q'}} \frac{1 - \rho^2_{c_p' c_r'} + \sqrt{\rho^2_{c_p' c_r'} \left(\rho^2_{c_p' c_r'} - 1 + \frac{\mathrm{WUE}^2 \, \sigma^2_{q'}}{\sigma^2_{c_p'}} \right)}}{1 - \rho^2_{c_p' c_r'} \pm \sqrt{\rho^2_{c_p' c_r'} \left(\rho^2_{c_p' c_r'} - 1 + \frac{\sigma^2_{c'}}{\sigma^2_{c_p'}} \right)}} \qquad \text{(A.1)}$$

where WUE is the water use efficiency on leaf-level (defined as negative), which can be estimated with Equation 4, $\overline{w'q'}$ and $\overline{w'c'}$ are the measured H_2O and CO_2 flux of the regarded time period, ρ and σ^2 are the correlation and variance of the indicated scalars (subscribes q, c, c_p, c_r represent H_2O, CO_2, photosynthesis, and R_s, respectively). The two parameters $\rho_{c_p'c_r'}$ and $\sigma_{c_p}{}^2$ in the equation are the only unknowns and the denominator implies two possible solutions, for what Palatella et al. (2014) implemented a globally convergent Newton's method searching for plausible solutions. As follows, we manipulated Equation A.1 further to solve for $\sigma_{c_p}{}^2 = f(\rho_{c_p'c_r'})$, leaving only $\rho_{c_p'c_r'}$ as unknown parameter, so that we could do without the numerical routine.

$$\mathrm{A} = \mathrm{WUE}^2 \left(\frac{\overline{w'q'}}{\overline{w'c'}} \right)^2 \left(2\,\rho^4_{c_p' c_r'} - 3\,\rho^2_{c_p' c_r'} + 1 \right) - \mathrm{WUE} \left(\frac{\overline{w'q'}}{\overline{w'c'}} \right) \left(2\,\rho^4_{c_p' c_r'} - 4\,\rho^2_{c_p' c_r'} + 2 \right) - \rho^2_{c_p' c_r'} + 1$$

$$B = 2\,WUE\left(\frac{\overline{w'q'}}{\overline{w'c'}}\right)\left(\mp\,WUE\left(\frac{\overline{w'q'}}{\overline{w'c'}}\right)\rho^2_{c'_p c'_r} \pm WUE\left(\frac{\overline{w'q'}}{\overline{w'c'}}\right) \pm \rho^2_{c'_p c'_r} \mp 1\right)$$

Only one branch of this equation is necessary, because B is always squared in the following equations. Both branches give the same solution for B^2.

$$C = WUE^2\,\rho^2_{c'_p c'_r}\left(\left(\frac{\overline{w'q'}}{\overline{w'c'}}\right)^2 \sigma^2_{c'} - \sigma^2_{q'}\right)$$

$$D = 2\,\frac{A\,C}{B^2} - \sigma^2_{c'}\,\rho^2_{c'_p c'_r}$$

$$E = \frac{A^2}{B^2} - \rho^4_{c'_p c'_r} + \rho^2_{c'_p c'_r}$$

$$\sigma^2_{c'_p\,1,2} = -\frac{1}{2}\frac{D}{E} \pm \sqrt{\left(\frac{1}{2}\frac{D}{E}\right)^2 - \frac{C^2}{B^2\,E}} \qquad \text{(A.2)}$$

B. Large Eddy Simulations

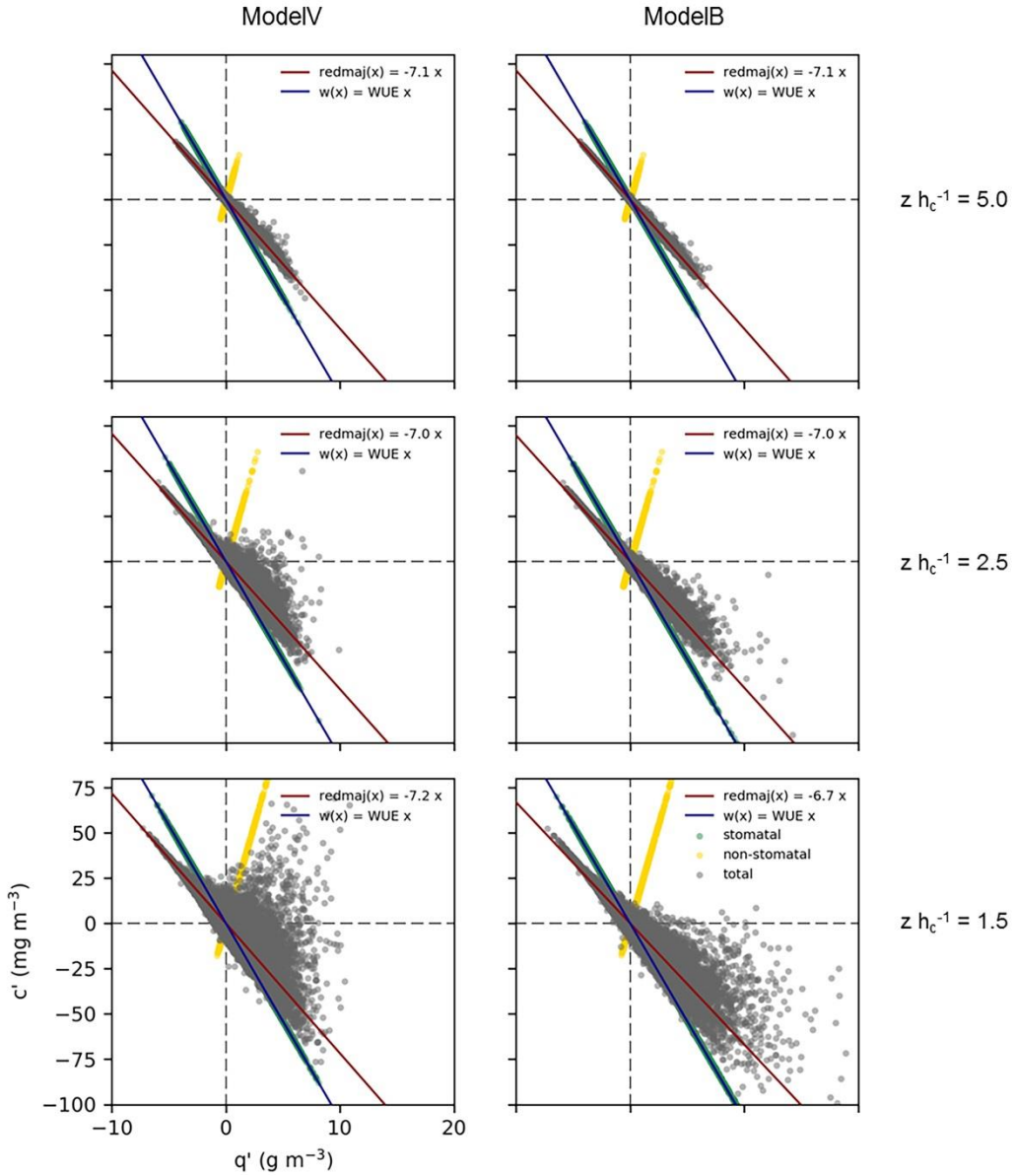

Fig. B.1: Examples of sampled synthetic high frequency data of H_2O (q') and CO_2 fluctuations (c') for the crop canopy in different 'measurement' heights and for the two sink-source-distributions ModelV (*left*) and ModelB (*right*) each with the strong soil source. In the LES-derived data it could be differentiated between scalars originating from stomatal (*green dots*) and non-stomatal (*yellow dots*) processes. The *blue line* presents the water use efficiency (WUE) and the *red line* the reduced major axis regression between total q' and c' (h_c: canopy height; z: height above soil surface).

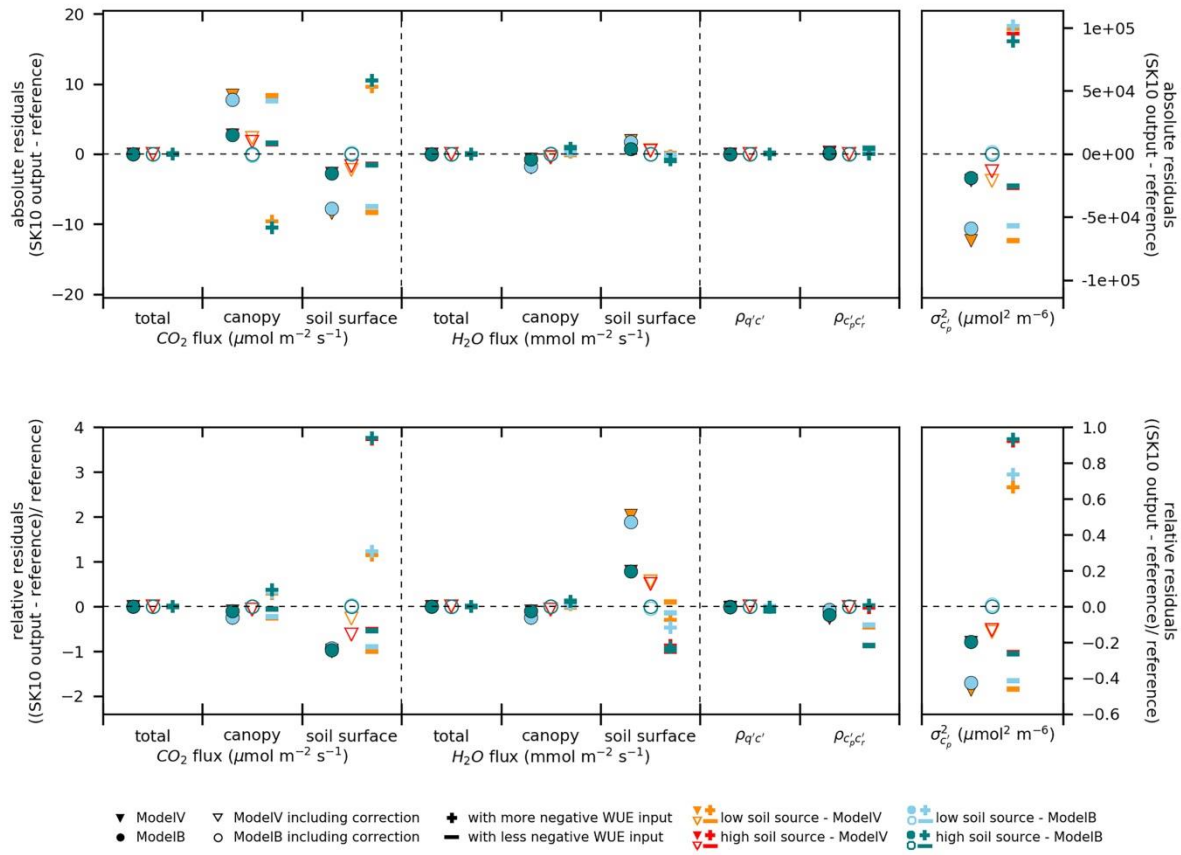

Fig. B.2: Absolute (*top*) and relative (*bottom*) residuals between H_2O and CO_2 flux components, $\rho_{q'c'}$, $\rho_{c_p'c_r'}$, and $\sigma_{c_p}^2$ resulting from LES scaled with the four variations of sink-source-distributions (ModelV or ModelB; low or high soil source) and the partitioning results of the approach after Scanlon and Kustas (2010, SK10) at a 'measurement' height of 2.5 canopy heights for the crop canopy. Shown are results of the partitioning procedure i) including correct water use efficiency (WUE) input known from LES, but without the correction of the transfer assumption (*filled markers*), ii) including correct WUE and corrected transfer assumption (*non-filled markers*), and iii) with corrected transfer assumption, but with a changed WUE of ±24% (*plus and minus signs*).